Consanguineous Families of Coordinated Carbon: A ReC_4Re Assembly That Is Isolable in Three Oxidation States, Including Crystallographically Characterized ReC≡CC≡CRe and $^{+}Re{=}C{=}C{=}C{=}C{=}Re^{+}$ Adducts and a Radical Cation in Which Charge Is Delocalized between Rhenium Termini

Monika Brady,[1] Weiqing Weng,[1] Yuanlin Zhou,[1] Jeffery W. Seyler,[1] Angelo J. Amoroso,[1] Atta M. Arif,[1] Marlis Böhme,[2] Gernot Frenking,*,[2] and J. A. Gladysz*,[1]

Contribution from the Department of Chemistry, University of Utah, Salt Lake City, Utah 84112, and the Fachbereich Chemie, Philipps-Universität Marburg, Hans-Meerwein-Strasse, D-35037 Marburg, Germany

Received September 10, 1996[⊗]

Abstract: Reaction of (η^5-C_5Me_5)Re(NO)(PPh_3)(C≡CH) and $Cu(OAc)_2$ (1.5 equiv, 80 °C, pyridine) gives the orange-brown ReC_4Re complex (η^5-C_5Me_5)Re(NO)(PPh_3)(C≡CC≡C)(Ph_3P)(ON)Re(η^5-C_5Me_5) (**2**, 88%) as a 50:50 diastereomer mixture. Crystallization affords (*SS*,*RR*)-**2**·$2CH_2Cl_2$ and solutions enriched in (*SR*,*RS*)-**2** (*meso*). Addition of $Ag^+PF_6^-$ (≥2 equiv) yields deep blue (*SS*,*RR*)- and (*SR*,*RS*)-$\mathbf{2}^{2+}2PF_6^-$ (86%), which give two geometric isomers (62:38, 89:11; CD_2Cl_2, −93 °C) about the $^{+}Re{=}C{=}C{=}C{=}C{=}Re^{+}$ linkages. Crystal structures of (*SS*,*RR*)-**2**·$2CH_2Cl_2$ and (*SS*,*RR*)-$\mathbf{2}^{2+}2PF_6^-$ show ReC_4Re units with bond angles (169−178°) and lengths (C≡C, 1.202(7); C−C 1.398(5); C=C 1.260−1.305(10) Å) near those of butadiyne or cumulenes. Natural bond order analysis and topological electron density calculations confirm the valence formulations. Reactions of (*SS*,*RR*)-**2** with (*SS*,*RR*)-$\mathbf{2}^{2+}2PF_6^-$ or $Ag^+PF_6^-$ (1 equiv) give a green radical cation (*SS*,*RR*)-$\mathbf{2}^{\bullet+}PF_6^-$ (μ = 1.74 μ_B; Faraday method). $E°$ data yield a K_c value of 1.1×10^9 (CH_2Cl_2, 22.5 °C) for the comproportionation. ESR spectra show undecets with $A_{iso,Re}$ values (98 G) half those of related monorhenium radical cations, indicating spin delocalization over two rheniums (I = 5/2). Accordingly, IR spectra give only one ν_{NO} band, positioned between those of **2** and $\mathbf{2}^{2+}2PF_6^-$ (CH_2Cl_2, 1665 vs 1623/1719 cm^{-1}). Near IR spectra show unique solvent-independent bands (883, 1000, 1200 nm; ϵ 15000, 9400, 3200 M^{-1} cm^{-1}). Sodium naphthalenide reduces (*SS*,*RR*)- or (*SR*,*RS*)-$\mathbf{2}^{\bullet+}PF_6^-$ to (*SS*,*RR*)- or (*SR*, *RS*)-**2**, establishing configurational stability. These and related data are analyzed in detail.

Numerous bimetallic complexes have been prepared in which the metals are linked by unsaturated ligands.[3] Among many attributes, the bridging moiety can mediate several types of charge transfer phenomena.[4] Some, such as photoinduced electron transfer[5] or hyperpolarizability,[6] are of potential practical importance. Others, such as electron delocalization in mixed valence compounds,[4,7] have considerable theoretical importance. Much effort has been directed at the "tuning" or optimization of these properties, which have received particular attention and speculation from the standpoints of nonlinear optics[6] and molecular devices such as wires and switches.[3,4,8]

We have been attracted to bimetallic complexes where the metals are linked by the most basic and fundamental class of unsaturated organic ligand—an sp carbon chain.[9] The development of such compounds, which have the general formula $L_nMC_xM'L'_{n'}$ (**I**), has lagged somewhat behind those with other types of unsaturated bridges.[3,7] However, they are now under intense study in numerous laboratories and relatively common for $x = 2$.[10,11] Furthermore, multiple redox states are possible, as exemplified for even carbon chains by **Ia**−**Ic** in Scheme 1. These differ by two electron increments and the numbers of bonds between the terminal carbons and endgroups. Both **Ia** and **Ic** have polyalkynyl chains with alternating single and triple bonds, whereas **Ib** has a cumulenic chain comprised of double bonds. Intermediate radical ions as well as alternative resonance forms or ground state valence formulations are also possible.

Scheme 1. Representative Redox States for Even Carbon Chain Complexes

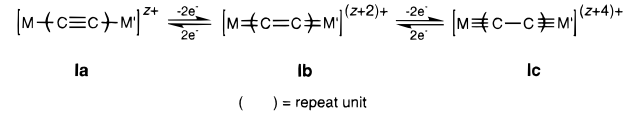

We have sought to synthesize a homologous series of complexes **I** with both short and long carbon chains and

[⊗] Abstract published in *Advance ACS Abstracts,* January 1, 1997.

(1) University of Utah.

(2) Philipps-Universität Marburg.

(3) Ward, M. D. *Chem. Soc. Rev.* **1995**, 121.

(4) Astruc, D. *Electron Transfer and Radical Processes in Transition Metal Chemistry*; VCH: New York, 1995; Part I.

(5) Some recent lead papers: (a) Lin, V. S.-Y.; DiMagno, S. G.; Therien, M. J. *Science* **1994**, *264*, 1105. (b) Sauvage, J.-P.; Collin, J.-P.; Chambron, J.-C.; Guillerez, S.; Coudret, C.; Balzani, V.; Barigelletti, F.; De Cola, L.; Flamigni, L. *Chem. Rev.* **1994**, *94*, 993.

(6) Long, N. J. *Angew. Chem., Int. Ed. Engl.* **1995**, *34*, 21.

(7) (a) Creutz, C. *Prog. Inorg. Chem.* **1983**, *30*, 1. (b) Crutchley, R. J. *Adv. Inorg. Chem.* **1994**, *41*, 273.

(8) See the following reviews, and references cited therein: (a) Ward, M. D. *Chem. Ind.* **1996**, 568. (b) Harriman, A.; Ziessel, R. *J. Chem. Soc., Chem. Commun.* **1996**, 1707.

(9) Lagow, R. J.; Kampa, J. J.; Wei, H.-C.; Battle, S. L.; Genge, J. W.; Laude, D. A.; Harper, C. J.; Bau, R.; Stevens, R. C.; Haw, J. F.; Munson, E. *Science* **1995**, *267*, 362.

(10) General reviews or perspectives: (a) Beck, W.; Niemer, B.; Wieser, M. *Angew. Chem., Int. Ed. Engl.* **1993**, *32*, 923. (b) Lang, H. *Angew. Chem., Int. Ed. Engl.* **1994**, *33*, 547. (c) Bunz, U. *Angew. Chem., Int. Ed. Engl.* **1996**, *35*, 969.

(11) Review of C_2 complexes: Akita, M.; Moro-oka, Y. *Bull. Chem. Soc. Jpn.* **1995**, *68*, 420.

S0002-7863(96)03181-2 CCC: $14.00

systematically characterize key structural, electronic, and chemical properties as functions of redox states and chain lengths.[12−15] These efforts have emphasized the sterically congested and strongly π donating chiral rhenium endgroup (η^5-C_5Me_5)Re(NO)(PPh_3) (**II**-Me_5), which carries 17 valence electrons as a neutral species. On the basis of data with other rigid bridging ligands,[16] we have operated under the premise that the shortest *even* carbon chain capable of spanning two such fragments would be four. Interestingly, recent data for sp carbon chains that bear *organic* endgroups suggest that there may be no practical upper limit on length[9]—an attractive scenario for possible device-like applications.

Surprisingly, when this study was launched, no complexes of the type **I** had been generated in more than one redox state.[12] However, neutral alkynyl (-C≡CR) and cationic vinylidene (=C=CRR′) complexes of **II**-Me_5—which can be viewed as monometallic analogs of **Ia** and **Ib**—had proven easily isolable.[16,17] Thus, we felt there was a good chance that sp carbon chains with **II**-Me_5 endgroups could be accessed in several redox states. Accordingly, the successful realization of this objective with C_4 bridges is detailed in the narrative below. These data also provide a baseline for companion studies that involve homologous C_6−C_{20} complexes[13] and analogs with bulkier and/or more electron releasing phosphines.[18]

Important complementary efforts with C_4−C_8 complexes of other metal fragments have appeared from several laboratories.[19,20] This work has been spearheaded by Lapinte, who has focused on the achiral and more electron releasing iron endgroup (η^5-C_5Me_5)Fe(dppe).[19] Much of his data were reported prior to or concurrently with our own. For comparative purposes, attempts have been made to record measurements under similar conditions in both laboratories. Furthermore, collaborations in progress have afforded C_x complexes that contain both iron and rhenium endgroups and will allow more perspicacious levels of comparisons.[21]

Scheme 2. Syntheses of Neutral and Dicationic ReC_4Re Complexes

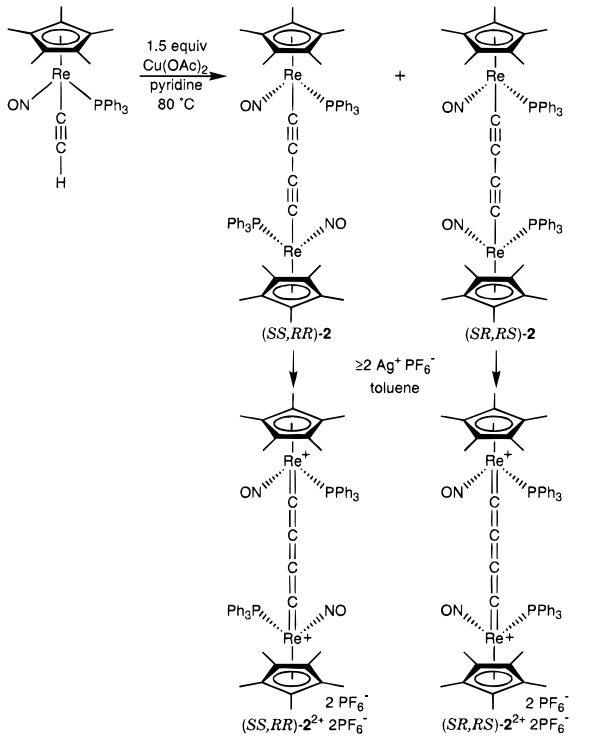

Results

1. μ-Butadiynediyl Complexes. Reaction of the chiral, racemic rhenium ethynyl complex (η^5-C_5Me_5)Re(NO)(PPh_3)(C≡CH) (**1**) and *n*-BuLi in THF at −80 °C gives the C_2Li complex (η^5-C_5Me_5)Re(NO)(PPh_3)(C≡CLi).[17] However, a variety of attempts to oxidatively couple this species were unsuccessful.[16] Thus, by analogy to well-known reactions of organic terminal alkynes,[22] the direct coupling of **1** was investigated. As shown in Scheme 2, **1** and $Cu(OAc)_2$ (1.5 equiv) were reacted in pyridine at 80 °C. Workup gave the air-stable, orange-brown μ-butadiynediyl complex (η^5-C_5Me_5)Re(NO)(PPh_3)(C≡CC≡C)(Ph_3P)(ON)Re(η^5-C_5Me_5) (**2**) in 88% yield. NMR spectra showed two closely spaced sets of signals, indicative of a 50:50 mixture of diastereomers. Crystallization from CH_2Cl_2/hexane gave the diastereomerically pure *dl* or "*rac*" solvate (*SS*,*RR*)-**2**·$2CH_2Cl_2$. Samples enriched in the *meso* diastereomer (*SR*,*RS*)-**2** were obtained from the supernatant. Isotopically labeled (*SS*,*RR*)-**2**-$^{13}C_4$ was similarly prepared, and diastereomer configurations were assigned crystallographically as described below.

Complex **2** was characterized by microanalysis, and NMR, IR, Raman, and UV/visible spectroscopy. Data are summarized in the Experimental Section, and many features are highlighted below. Low temperature ^{1}H or ^{31}P NMR spectra did not show any decoalescence phenomena (CD_2Cl_2, −80 °C; THF, −110 °C). The ^{13}C NMR signals of the C_4 chain were difficult to detect, but labeled (*SS*,*RR*)-**2**-$^{13}C_4$ gave intense resonances (ppm, C_6D_6) at 95.8 (ddd, $J_{CP}/^1J_{CC}/^2J_{CC}$ = 10.9/96.5/47.1 Hz) and 117.5 (dd, J_{CC}/J_{CC} = 97.2/47.6 Hz).[23] The former was assigned as the Re***C*** signal from the phosphorus coupling. For comparison, the ethynyl complex of **II**-Me_5 exhibits Re***C***≡***C*** signals

(12) Preliminary communications of this work: (a) Zhou, Y.; Seyler, J. W.; Weng, W.; Arif, A. M.; Gladysz, J. A. *J. Am. Chem. Soc*. **1993**, *115*, 8509. (b) Seyler, J. W.; Weng, W.; Zhou, Y.; Gladysz, J. A. *Organometallics* **1993**, *12*, 3802.

(13) (a) Brady, M.; Weng, W.; Gladysz, J. A. *J. Chem. Soc., Chem. Commun*. **1994**, 2655. (b) Bartik, T.; Bartik, B.; Brady, M.; Dembinski, R.; Gladysz, J. A. *Angew. Chem., Int. Ed. Engl.* **1996**, *35*, 414. (c) Bartik, B.; Dembinski, R.; Bartik, T.; Arif, A. M.; Gladysz, J. A. *New J. Chemistry* **1997**, in press.

(14) Weng, W.; Bartik, T. ; Brady, M.; Bartik, B.; Ramsden, J. A.; Arif, A. M.; Gladysz, J. A. *J. Am. Chem. Soc.* **1995**, *117*, 11922.

(15) (a) Weng, W.; Ramsden, J. A.; Arif, A. M.; Gladysz, J. A. *J. Am. Chem. Soc*. **1993**, *115*, 3824. (b) Weng, W.; Bartik, T.; Gladysz, J. A. *Angew. Chem., Int. Ed. Engl*. **1994**, *33*, 2199.

(16) Weng, W.; Bartik, T.; Johnson, M. T.; Arif, A. M.; Gladysz, J. A. *Organometallics* **1995**, *14*, 889.

(17) Ramsden, J. A.; Weng, W.; Gladysz, J. A. *Organometallics* **1992**, *11*, 3635.

(18) Meyer, W. E.; Amoroso, A. J.; Gladysz, J. A., work in progress.

(19) (a) Le Narvor, N.; Lapinte, C. *J. Chem. Soc., Chem. Commun*. **1993**, 357. (b) Le Narvor, N.; Toupet, L.; Lapinte, C. *J. Am. Chem. Soc*. **1995**, *117*, 7129. (c) Coat, F.; Lapinte, C. *Organometallics* **1996**, *15*, 477.

(20) Other $L_nMC_4M'L'_{n'}$ complexes: (a) Sonogashira, K.; Kataoka, S.; Takahashi, S.; Hagihara, N. *J. Organomet. Chem*. **1978**, *160*, 319. (b) Wong, A.; Kang, P. C. W.; Tagge, C. D.; Leon, D. R. *Organometallics* **1990**, *9*, 1992. (c) Fyfe, H. B.; Mlekuz, M.; Zargarian, D.; Taylor, N. J.; Marder, T. B. *J. Chem. Soc., Chem. Commun*. **1991**, 188. (d) Stang, P. J.; Tykwinski, R. *J. Am. Chem. Soc*. **1992**, *114*, 4411. (e) Crescenzi, R.; Sterzo, C. L. *Organometallics* **1992**, *11*, 4301. (f) Rappert, T.; Nürnberg, O.; Werner, H. *Organometallics* **1993**, *12*, 1359. (g) Bruce, M. I.; Hinterding, P.; Tiekink, E. R. T.; Skelton, B. W.; White, A. H. *J. Organomet. Chem*. **1993**, *450*, 209. (h) Yam, V. W.-W.; Lau, V. C.-Y.; Cheung, K.-K. *Organometallics* **1996**, *15*, 1740. (i) Gevert, O.; Wolf, J.; Werner, H. *Organometallics* **1996**, *15*, 2806. (j) Viola, E.; Lo Sterzo, C.; Trezzi, F. *Organometallics* **1996**, *15*, 4352.

(21) Lapinte, C.; Gladysz, J. A.; Paul, F.; Meyer, W. E., work in progress.

(22) Eglinton, G.; McCrae, W. *Adv. Org. Chem*. **1963**, *4*, 225.

(23) The $^1J_{CC}$ values of the ReC_4Re carbons of (*SS*,*RR*)-**2** and (*SS*,*RR*)-$\mathbf{2}^{2+}2PF_6^-$ are much smaller than in organic model compounds such as butadiyne and butatriene, presumably due to enhanced s character in the orbitals used for σ bonding to the electropositive rhenium. For related examples and further analysis, see: Caulton, K. G.; Cayton, R. H.; Chisholm, M. H.; Huffman, J. C.; Lobkovsky, E. B.; Xue, Z. *Organometallics* **1992**, *11*, 321 (Table V).

Table 1. Summary of IR and Raman Data (cm^{-1})

compd[a]	medium	IR ν_{NO}	IR ν_{CC}	Raman ν_{CC}[b]
2	CH_2Cl_2	1623 s	1964 w	2056 s
	KBr	1629 s br	1968 w	
	CH_3CN	1629 s	1967 w	
	THF	1630 s	1967 w	
2-$^{13}C_4$	CH_2Cl_2	1624 s	1888[c] w	
$\mathbf{2}^{\bullet+}PF_6^-$	CH_2Cl_2	1665 s	1872 m	1990 s
	KBr	1654 s br	1870 m	
	CH_3CN	1665 s	1872 m	
	THF	1668 s	1871 m	
$\mathbf{2}^{\bullet+}$-$^{13}C_4$ PF_6^-	CH_2Cl_2	1668 s	1799[d] m	
	KBr	1655 s	1799 m	
$\mathbf{2}^{2+}2PF_6^-$	CH_2Cl_2	1719 s	not obs.	1883 s
	KBr	1692 s br	not obs.	
	CH_3CN	1725 s	not obs.	
$\mathbf{2}^{2+}$-$^{13}C_4$ $2PF_6^-$	CH_2Cl_2	1712 s	not obs.	

[a] *SS,RR* and *SR,RS* diastereomers gave identical spectra. [b] Raman spectra did not show ν_{NO} bands. [c] Calculated, 1887. [d] Calculated, 1799.

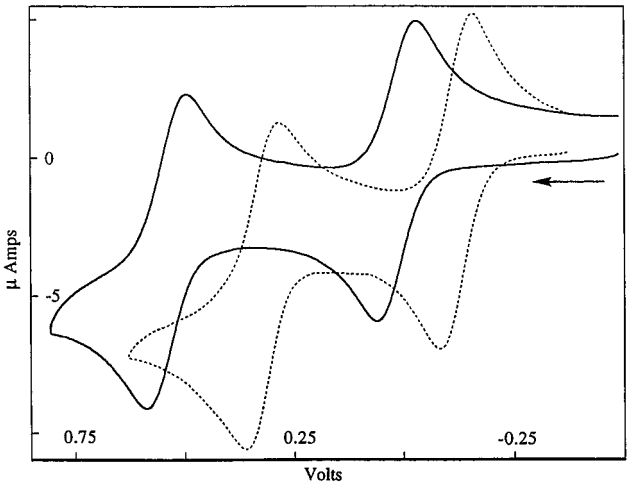

Figure 1. Cyclic voltammograms of (*SS,RR*)-**2** (100 mV/s): solid trace, 2×10^{-3} M in 0.1 M *n*-$Bu_4N^+BF_4^-/CH_2Cl_2$, E°′(ferrocene) = 0.46 V;[25] dashed trace, 3×10^{-3} M in 0.1 M $Et_4N^+ClO_4^-/CH_3CN$, *E*°′-(ferrocene) = 0.38 V.[25]

at 98.0 (d, J_{CP} = 15.8 Hz) and 116.0 (s).[17] IR spectra showed $\upsilon_{C\equiv C}$ and υ_{NO} bands as summarized in Table 1. A Raman spectrum gave an intense $\upsilon_{C\equiv C}$ band at higher frequency (Δcm^{-1} 92) but no υ_{NO} band. With (*SS,RR*)-**2**-$^{13}C_4$, the isotopically shifted $\upsilon_{C\equiv C}$ band (Δcm^{-1} 76) was within 1 cm^{-1} of the calculated value.

Cyclic voltammograms of (*SS,RR*)-**2** were recorded in CH_3CN and CH_2Cl_2 as described in Figure 1 and the Experimental Section. Two chemically reversible one electron oxidations occurred.[24] Depending upon convention,[25] the $E°_1$ and $E°_2$ values were +0.06 and +0.50 V or −0.12 and +0.32 V in CH_3CN (ΔE_p 60 mV), and +0.11 and +0.64 V or +0.01 and +0.54 V in CH_2Cl_2 (ΔE_p 90 mV). In all cases, the i_a/i_c ratio was unity. No reductions were observed out to the solvent-imposed cathodic limits of −0.7 and −1.1 V (or −0.9 and −1.2 V).[25b] Thus, the corresponding radical cation (*SS,RR*)-$\mathbf{2}^{\bullet+}X^-$ and dication (*SS,RR*)-$\mathbf{2}^{2+}2X^-$ were viewed as feasible targets for synthesis. The preparation of the latter, which was anticipated to be diamagnetic, was attempted first.

2. μ-Butatrienediylidene Complexes. As shown in Scheme 2, (*SS,RR*)-**2** and $Ag^+PF_6^-$ (2.5 equiv) were combined in toluene. Workup gave the air stable, deep blue, analytically pure μ-butatrienediylidene complex (*SS,RR*)-$\mathbf{2}^{2+}2PF_6^-$ in 86% yield. The labeled complex (*SS,RR*)-$\mathbf{2}^{2+}$-$^{13}C_4$ $2PF_6^-$, and samples enriched in the *meso* diastereomer (*SR,RS*)-$\mathbf{2}^{2+}2PF_6^-$, were similarly prepared. All compounds were characterized analogously to **2**. The ^{13}C NMR spectrum of (*SS,RR*)-$\mathbf{2}^{2+}$-$^{13}C_4$ $2PF_6^-$ showed a characteristic downfield Re═***C*** signal (ppm, CD_2Cl_2) at 305.1 (ddd, $J_{CP}/^1J_{CC}/^2J_{CC}$ = 12.3/77.0/40.7 Hz) and a Re═C═***C*** signal at 213.5 (dd, $^1J_{CC}/^2J_{CC}$ = 77.0/40.7 Hz).[23] For comparison, the vinylidene complex of **II**-Me_5 exhibits Re═***C***═***C***H_2 signals at 330.4 (d, J_{CP} = 9.5 Hz) and 111.6 (s).[16] The IR υ_{NO} value (Table 1) was much greater than that of **2**, consistent with reduced backbonding. No cumulenic IR υ_{CC} bands were detected, but an intense Raman absorption occurred at 1883 cm^{-1}.

Unsymmetrically-substituted alkylidene and vinylidene complexes of **II**-Me_n give geometric isomers that differ in the orientation of the ═CRR′ termini and interconvert with barriers of 18−21 kcal/mol.[16,17,26,27] Crystal structures establish Re═C conformations that allow high degrees of overlap of the carbon fragment p acceptor orbitals and the rhenium fragment d-type HOMO. These are illustrated by the idealized Newman-type projections **III** (alkylidene) and **IV** (vinylidene) in Scheme 3.[28] It can similarly be derived that (*SS,RR*)- and (*SR,RS*)-$\mathbf{2}^{2+}2PF_6^-$ should give geometric isomers of structures **V**/**VI** and **VII**/**VIII**, respectively.[28] Accordingly, when ^{31}P NMR spectra were recorded in CD_2Cl_2 at −93 °C, *two* resonances were observed for each diastereomer (*SS,RR*: 26.8/28.4 ppm, 62:38; *SR,RS*: 26.1/28.2 ppm, 89:11). Representative spectra are shown in Figure 2.

Consider the case of (*SS,RR*)-$\mathbf{2}^{2+}2PF_6^-$. The bulky PPh_3 ligands on each terminus are *anti* in **V** but *syn* in **VI**. Therefore, **V** and **VI** are assigned as the major and minor geometric isomers, respectively. With (*SR,RS*)-$\mathbf{2}^{2+}2PF_6^-$, **VII** allows a staggered arrangement of the three ligands on each terminus, with the PPh_3 (and pentamethylcyclopentadienyl) groups *anti*. However, **VIII** enforces an eclipsed arrangement of the ligands on each terminus, with the PPh_3 (and pentamethylcyclopentadienyl) groups *syn*. Thus, **VII** and **VIII** are assigned as the major and minor isomers. They would logically have a greater free energy difference than **V** and **VI**, consistent with the increased isomer ratio. Hence, there is an appreciable degree of steric communication across the C_4 chain.

When NMR samples were warmed, the ^{31}P resonances markedly shifted and broadened, as shown in Figure 2. The *SS,RR* and *SR,RS* diastereomers gave only one signal above −22 and −5 °C, respectively. However, at higher temperatures (32, 42, 47 °C), the peaks did not significantly sharpen. For comparison, variable temperature NMR spectra of (*SS,RR*)-**2** were similarly recorded. Between −50 and −10 °C, the ^{31}P

(24) The *SS,RR* diastereomer and samples enriched in the *SR,RS* diastereomer gave identical data.

(25) (a) To date, all *E*° values from our laboratory have been consistently reported relative to a ferrocene *E*°′ value of 0.56 V.[12b,13a,b,14] A recent authoritative review[25d] has proposed protocols for standardizing *E*° values from a variety of solvent/electrolyte combinations to a common SCE reference. These employ ferrocene *E*°′ values of 0.38 V in CH_3CN/*n*-$Bu_4N^+ClO_4^-$ and 0.46 V in CH_2Cl_2/*n*-$Bu_4N^+PF_6^-$.[25d] In order to facilitate comparisons of our *E*° values with others in the literature, this convention (utilized for Figure 1) will be adopted henceworth. Revised values for data reported elsewhere[13a,b,14] will be given in future full papers. (b) Revised $E°_1$ and $E°_2$ values for **2** are thereby −0.12 and 0.32 V in CH_3CN and 0.01 V and 0.54 V in CH_2Cl_2. (c) The $E°_1$ and $E°_2$ values reported for the FeC_4-Fe complex **3** (−0.675 and 0.045 V, CH_2Cl_2/*n*-$Bu_4N^+PF_6^-$) are relative to a ferrocene *E*°′ value of 0.420 V,[19] and therefore closely comparable to those in (b). (d) Connelly, N. G.; Geiger, W. E. *Chem. Rev.* **1996**, *96*, 877.

(26) NMR data bound the Re═C rotational barrier in the methylidene complex of **II**-Me_5 as > 19 kcal/mol (114 °C): Patton, A. T.; Strouse, C. E.; Knobler, C. B.; Gladysz, J. A. *J. Am. Chem. Soc.* **1983**, *105*, 5804.

(27) Data for adducts of **II**-Me_0: (a) Senn, D. R.; Wong, A.; Patton, A. T.; Marsi, M.; Strouse, C. E.; Gladysz, J. A. *J. Am. Chem. Soc.* **1988**, *110*, 6096. (b) Kiel, W. A.; Lin, G.-Y.; Constable, A. G.; McCormick, F. B.; Strouse, C. E.; Eisenstein, O.; Gladysz, J. A. *J. Am. Chem. Soc.* **1982**, *104*, 4865. (c) Kowalczyk, J. J.; Arif, A. M.; Gladysz, J. A. *Chem. Ber.* **1991**, *124*, 729 and references therein.

(28) The P−Re−N bond angles in **III**−**VIII** are 90°, consistent with the formally octahedral nature of these complexes, and much crystallographic data.[27]

Scheme 3. Relationship between the HOMO of the Rhenium Fragment **II**$^{+}$-Me$_n$ and Conformations of Alkylidene (**III**), Vinylidene (**IV**), and μ-Butatrienediylidene (**V**−**VIII**) Adducts

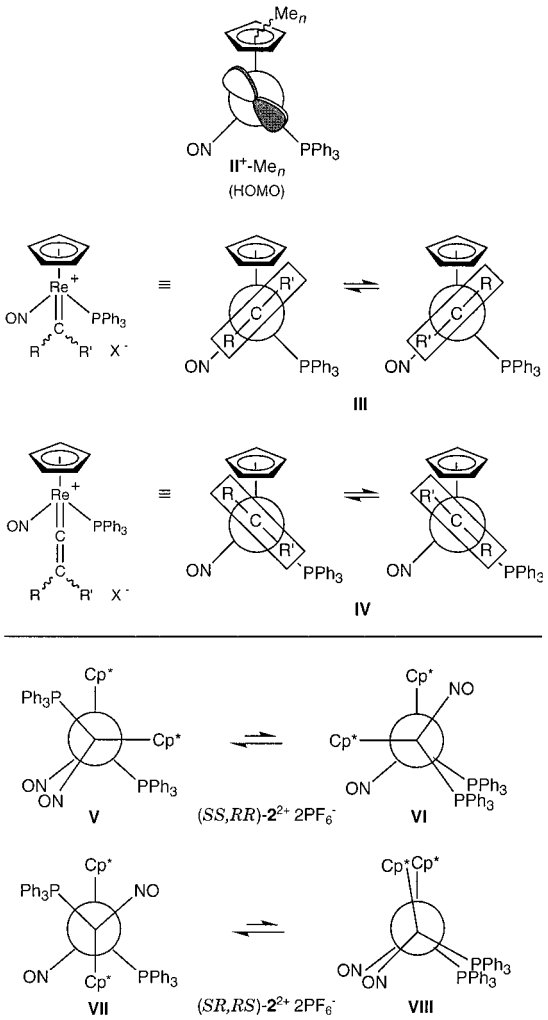

resonance shifted by 16.6 Hz (0.12 ppm), whereas those of (*SS*,*RR*)-**2**$^{2+}$2PF$_6^-$ shifted by 71.9 and 152.5 Hz (0.59 and 1.26 ppm). Interestingly, the pentamethylcyclopentadienyl ^{1}H resonances shifted by comparable amounts (19.7 vs 19.4 Hz, −50 to −20 °C).

We were concerned that **2**$^{2+}$2PF$_6^-$ might have a low-lying, biradical-like, triplet excited state ($S = 1$). Such equilibria are commonly temperature dependent, and evidenced by marked changes in NMR chemical shifts.[29] Furthermore, Lapinte's data for a related FeC$_4$Fe complex (below) suggest a very close and possibly inverted singlet/triplet energy spacing.[19a,b] However, **2**$^{2+}$2PF$_6^-$ did not give a detectable ESR signal (CH_2Cl_2), and other probes described below gave similarly negative results. Hence, we provisionally interpret Figure 2 as reflecting two consecutive coalescences ($\Delta G^{\ddagger}(T_c) \approx 11.6-11.9$ and 12.3−13.5 kcal/mol)[30] involving resonances and underlying equilibria that are highly temperature dependent.

3. Crystal Structures. The crystal structures of (*SS*,*RR*)-**2**·2CH_2Cl_2 and (*SS*,*RR*)-**2**$^{2+}$2PF$_6^-$ were determined as outlined in Table 2 and the Experimental Section. With the latter, data were acquired at −100 °C. Results of an ambient temperature (16 °C) structure determination were reported in our original communication.[12a] Key bond lengths, bond angles, and plane/plane angles are listed in Table 3. For (*SS*,*RR*)-**2**·2CH_2Cl_2, the ReC$_4$Re midpoint is coincident with a crystallographic inversion center, giving equivalent rhenium termini. As shown in Figures 3 and 4, both compounds have nearly linear ReC$_4$Re moieties, with Re−C−C and C−C−C bond angles ranging from 169° to 178°.

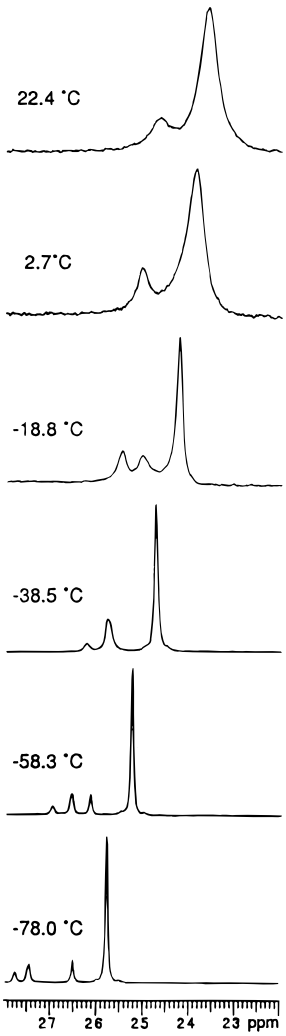

Figure 2. Variable temperature $^{31}P\{^1H\}$ NMR spectra of a 17:83 mixture of (*SS*,*RR*)-**2**$^{2+}$2PF$_6^-$ and (*SR*,*RS*)-**2**$^{2+}$2PF$_6^-$ in CD_2Cl_2.

Complex (*SS*,*RR*)-**2** exhibits C≡C and C−C bond lengths (1.202(7), 1.389(5) Å) very close to those in butadiyne (1.218(2), 1.384(2) Å)[31] and three other structurally characterized MC≡CC≡CM species (M = Ru/Re/Rh: 1.217(4)/1.19(2)/1.205(5), 1.370(6)/1.43(4)/1.388(7) Å).[20g,h,i] The Re−C bond length (2.037(5) Å) is similar to those in other C≡CX adducts of **II**-Me$_5$ (2.079(9), 2.032(7) Å).[13c,14] Complex (*SS*,*RR*)-**2**$^{2+}$2PF$_6^-$ exhibits Re═C bond lengths (1.909(7)/1.916(7) Å) close to that in a related compound with a $^+$Re═C═C═C═Mn linkage (1.91(1) Å).[15a] The C═C bond lengths (1.263(10)/1.260(10), 1.305(10) Å) are near those of butatriene (1.283(5)−1.318(5) Å) and the one hexapentaene that has been structurally characterized to date (1.259−1.339 Å).[32]

As shown graphically in Figure 4 (bottom), the C═C bond lengths in these compounds give alternating short/long patterns.

(29) (a) Kriley, C. E.; Fanwick, P. E.; Rothwell, I. P. *J. Am. Chem. Soc.* **1994**, *116*, 5225. (b) Cotton, F. A.; Eglin, J. L.; Hong, B.; James, C. A. *J. Am. Chem. Soc.* **1992**, *114*, 4915. (c) Hopkins, M. D.; Zietlow, T. C.; Miskowski, V. M.; Gray, H. B. *J. Am. Chem. Soc.* **1985**, *107*, 510.

(30) Sandström, J. *Dynamic NMR Spectroscopy*; Academic Press: New York, 1982.

(31) Tanimoto, M.; Kuchitsu, K.; Morino, Y. *Bull. Chem. Soc. Jpn.* **1971**, *44*, 386.

(32) (a) Almenningen, A.; Bastiansen, O.; Trætteberg, M. *Acta Chem. Scand.* **1961**, *15*, 1557. (b) Irngartinger, H.; Götzmann, W. *Angew. Chem., Int. Ed. Engl.* **1986**, *25*, 340. (c) See, also: Morimoto, Y.; Higuchi, Y.; Wakamatsu, K.; Oshima, K.; Utimoto, K.; Yasuoka, N. *Bull. Chem. Soc. Jpn.* **1989**, *62*, 639.

Table 2. Summary of Crystallographic Data for (*SS*,*RR*)-**2**·$2CH_2Cl_2$ and (*SS*,*RR*)-$\mathbf{2}^{2+}2PF_6^-$

molecular formula	$C_{62}H_{64}Cl_4N_2O_2P_2Re_2$	$C_{60}H_{60}F_{12}N_2O_2P_4Re_2$
molecular weight	1445.374	1565.436
crystal system	monoclinic	monoclinic
space group	C_2/c	$P2_1/c$
temp of collection (°C)	16	−100
cell dimensions		
a, Å	26.898(8)	17.388(6)
b, Å	11.437(3)	20.484(3)
c, Å	19.613(4)	17.411(4)
β, deg	95.172(2)	108.12(2)
V, Å^3	6008.97	5894(3)
Z	4	4
d_{calc}, g/cm^3	1.598	1.764
d_{found}, g/cm^3 (22 °C)	1.602	1.734
crystal dimensions, mm	0.33 × 0.31 × 0.28	0.31 × 0.28 × 0.25
diffractometer	CAD4	CAD4
radiation (Å)	Mo K_α(0.70930)	Mo K_α(0.70930)
data collection method	$\theta-2\theta$	$\theta-2\theta$
scan speed, deg/min	variable	variable
reflections measured	5697	10707
range/indices (*j*,*k*,*l*)	0 31, 0 11, −23, 22	0 20, 0 24, −20 19
2θ limit, deg	4.0−50.0	4.5−50.0
scan width	0.80 + 0.34 tan θ	0.80 + 0.34 tan θ
std reflections	1 X-ray hour	1 X-ray hour
total unique data	5568	10337
obsd data, $I > 3\sigma(I)$	3878	
abs. coefficient, cm^{-1}	43.54	42.95
min. transmission, %	89.8	79.8
max. transmission, %	99.9	99.9
no. of variables	334	749
goodness of fit	1.232	1.131
$R = \sum\|\|F_o\| - \|F_c\|\|/\sum\|F_o\|$	0.0291	0.0380 (R1, 2σ)
$R_w = \sum\|\|F_o\| - \|F_c\|\|w^{1/2}/\sum\|F_o\|\|w^{1/2}$	0.0370	
$wR2 = (\sum[\mathbf{w}(F_o^2 - F_c^2)^2]/\sum[wF_o^4])^{1/2}$		0.0861
Δ/σ (max)	0.008	0.001
Δ/ρ (max), e/Å^3	0.652	1.343 (ca. 1.095 Å from Re1)

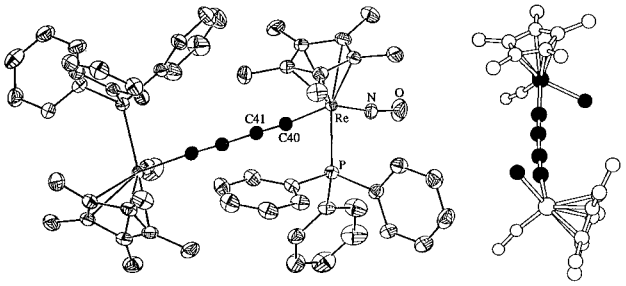

Figure 3. Full (left) and partial (right) molecular structure of (*SS*,*RR*)-**2**·$2CH_2Cl_2$.

This is well documented for butatrienes, where the interior sp/sp C═C bond is shorter than the terminal sp/sp^2 C═C bonds.[32] However, the interior sp/sp C═C bonds of the hexapentaene also vary appreciably.[32b] Interestingly, (*SS*,*RR*)-$\mathbf{2}^{2+}2PF_6^-$ gives a pattern opposite to that of butatriene but analogous to the hexapentaene.[33] Since the hexapentaene has the same number of sp carbons and π bonds as $\mathbf{2}^{2+}2PF_6^-$, it likely constitutes a better structural model. Computational data and further analyses are presented below.

The ReC_4Re linkages in (*SS*,*RR*)-**2** and (*SS*,*RR*)-$\mathbf{2}^{2+}2PF_6^-$ contain the same number of σ bonds (five) but different numbers of π bonds (four vs five). Accordingly, the rhenium−rhenium distance contracts from 7.8288(4) to 7.6350(8) Å upon oxidation (16 °C values), despite the potential for electrostatic repulsion. The angle of the P−Re−C planes about the electronically unconstrained C≡CC≡C bridge in (*SS*,*RR*)-**2** is 148° (Figure 3), giving an approximately *anti* arrangement of the bulky PPh_3 ligands and a plausible steric energy minimum. However, the corresponding angle in (*SS*,*RR*)-$\mathbf{2}^{2+}2PF_6^-$ is 23° (Figure 4), placing the PPh_3 ligands *syn* as in the less stable idealized geometric isomer **VI** (Scheme 3). An *anti* orientation, as in **V**, would have also been consistent with a purely steric energy minimum. Thus, the contrasteric arrangement provides further evidence for the electronic conformation-determining factors

(33) Since the C═C bond lengths in (*SS*,*RR*)-$\mathbf{2}^{2+}2PF_6^-$ are within three esd values of each other, it can be questioned whether they are statistically different. However, note that the trend is reproduced in two independent determinations (footnote a, Table 3).

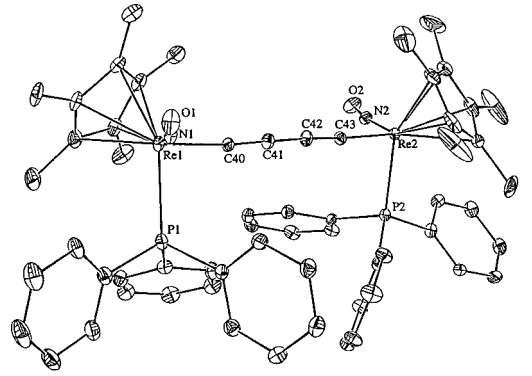

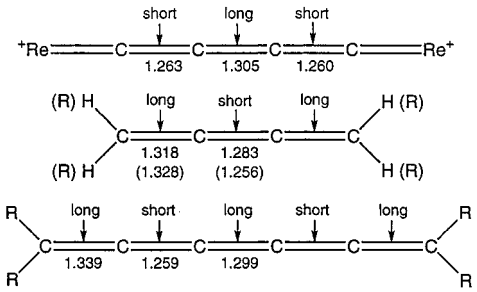

Figure 4. Structure of the dication of (*SS*,*RR*)-$\mathbf{2}^{2+}2PF_6^-$ and comparisons with organic cumulenes.

Table 3. Selected Bond Lengths (Å), Bond Angles (deg), and Plane−Plane Angles (deg) in (*SS*,*RR*)-**2**·$2CH_2Cl_2$ and (*SS*,*RR*)-$\mathbf{2}^{2+}2PF_6^-$

(*SS*,*RR*)-**2**·$2CH_2Cl_2$			
Re−P	2.375(1)	Re−Cp* centroid	1.964
Re−N	1.754(5)	P−C11	1.831(6)
Re−C40	2.037(5)	P−C21	1.830(6)
C40−C41	1.202(7)	P−C31	1.833(6)
C41−C41′	1.389(5)	N−O	1.190(6)
N−Re−C40	100.7(2)	Re−C40−C41	174.4(5)
P−Re−C40	82.4(1)	C40−C41−C41′	176.8(6)
P−Re−N	92.8(2)	Re−N−O	170.9(6)
Re−P−C40/ Re′−P′−C40′	148.4(1)	Re−C40−N/ Re′−C40′−N′	25.2(1)
(*SS*,*RR*)-$\mathbf{2}^{2+}2PF_6^-$			
Re1−P1	2.439(2)	Re1−Cp* centroid	1.972
Re2−P2	2.430(2)	Re2−Cp* centroid	1.963
Re1−N1	1.777(6)	P1−C11	1.811(8)
Re2−N2	1.767(6)	P1−C21	1.815(8)
Re1−C40[a]	1.909(7)	P1−C31	1.816(7)
Re2−C43[a]	1.916(7)	P2−C61	1.813(7)
C40−C41[a]	1.263(10)	P2−C71	1.813(8)
C41−C42[a]	1.305(10)	P2−C81	1.821(7)
C42−C43[a]	1.260(10)	N1−O1	1.179(8)
		N2−O2	1.184(8)
N1−Re1−C40	103.2(3)	Re1−C40−C41	168.5(7)
N2−Re2−C43	101.7(3)	Re2−C43−C42	171.4(7)
P1−Re1−C40	88.6(2)	C40−C41−C42	177.8(9)
P2−Re2−C43	92.4(2)	C41−C42−C43	175.4(9)
P1−Re1−N1	93.7(2)	Re1−N1−O1	167.8(6)
P2−Re2−N2	87.7(2)	Re2−N2−O2	171.7(6)
Re1−C40−P1/ Re2−C43−P2	22.5(2)	Re1−C40−P1/ Re2−C43−N2	70.9(2)
Re1−N1−C40/ Re2−C43−P2	66.2(2)	Re1−N1−C40/ Re2−C43−N2	22.8(2)

[a] The following values were obtained from a second, room temperature structure:[12a] Re1−C40 1.93(1), Re2−C43 1.91(1), C40−C41 1.24(2), C41−C42 1.33(2), C42−C43 1.26(2).

invoked in Scheme 3. It is presumably a fortuitous consequence of the kinetics of crystallization.

4. Isolation and Reduction of a Radical Cation. From the above $E°$ data, equilibrium constants were calculated for the *com*proportionation of (*SS*,*RR*)-**2** and (*SS*,*RR*)-$\mathbf{2}^{2+}2X^-$ to the radical cation (*SS*,*RR*)-$\mathbf{2}^{\bullet+}X^-$ (K_c).[34] The values were very large, ranging from 1.1×10^9 (CH_2Cl_2, 22.5 °C) to 2.1×10^7 (CH_3CN, 22.5 °C). Thus, as shown in Scheme 4, (*SS*,*RR*)-**2** and (*SS*,*RR*)-$\mathbf{2}^{2+}2PF_6^-$ were combined in CH_2Cl_2. Workup gave (*SS*,*RR*)-$\mathbf{2}^{\bullet+}PF_6^-$ as a deep green, analytically pure powder in 50% yield. The reaction of (*SS*,*RR*)-**2** and $Ag^+PF_6^-$ (1.0 equiv) in toluene also gave (*SS*,*RR*)-$\mathbf{2}^{\bullet+}PF_6^-$ (69%). The labeled complex (*SS*,*RR*)-$\mathbf{2}^{\bullet+}$-$^{13}C_4$ PF_6^- and samples enriched in the *meso* diastereomer (*SR*,*RS*)-$\mathbf{2}^{\bullet+}PF_6^-$ were similarly prepared.

As a solid, (*SS*,*RR*)-$\mathbf{2}^{\bullet+}PF_6^-$ was stable for weeks under an inert atmosphere and decomposed with melting at 108−111 °C. In contrast, degassed CH_2Cl_2 or CH_3CN solutions showed some decomposition after several hours at room temperature. An inhomogeneous, deeper green material formed.[35] Extensive efforts to grow crystals of (*SS*,*RR*)-$\mathbf{2}^{\bullet+}PF_6^-$ suitable for X-ray studies were unsuccessful. Thus, the hexafluoroantimonate salt (*SS*,*RR*)-$\mathbf{2}^{\bullet+}SbF_6^-$ was prepared utilizing $Ag^+SbF_6^-$. Slow

Scheme 4. Syntheses of a Paramagnetic ReC_4Re Complex

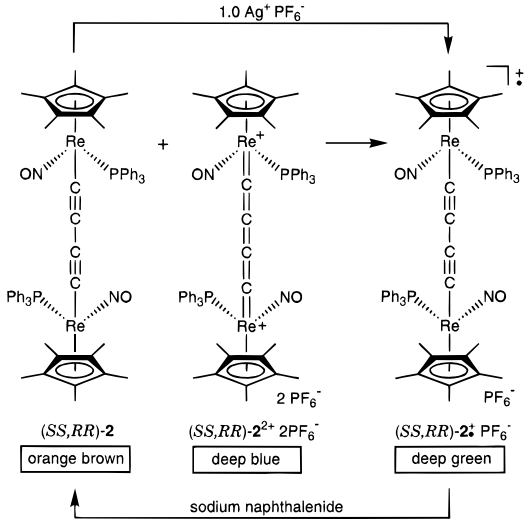

crystallizations from CH_2Cl_2/hexane at low temperatures gave green needles. However, they were soft, fractured easily, and diffracted poorly. Crystallizations involving a variety of other chlorinated solvents were less successful.

Complex (*SS*,*RR*)-$\mathbf{2}^{\bullet+}PF_6^-$ gave a cyclic voltammogram equivalent to that of (*SS*,*RR*)-**2**. We sought to probe its configurational stability, especially in view of evidence suggesting the rapid inversion of chiral iron radical cations of the formula $[(\eta^5\text{-}C_5H_5)Fe(CO)(L)(CH_3)]^{\bullet+}$.[36] Since direct methods for assaying diastereomeric purity were not apparent, a chemical cycle was utilized. First, CH_2Cl_2 solutions of (*SS*,*RR*)-$\mathbf{2}^{\bullet+}PF_6^-$ and samples enriched in (*SR*,*RS*)-$\mathbf{2}^{\bullet+}PF_6^-$ were stirred for 4 h in the dark. Then sodium naphthalenide was added. Workup gave **2** in 72% yield. NMR analyses (^1H, ^{31}P) showed diastereomer ratios that were identical with those of the samples of **2** originally used to prepare $\mathbf{2}^{\bullet+}PF_6^-$. Hence, $\mathbf{2}^{\bullet+}PF_6^-$ does not readily epimerize in solution, and configuration must be retained for all reactions in Scheme 4.

5. Magnetic and Optical Properties. The corrected molar magnetic susceptibility of (*SS*,*RR*)-$\mathbf{2}^{\bullet+}PF_6^-$, χ_M, was determined by the Faraday method.[37] As shown in Figure 5, a plot of χ_M^{-1} vs temperature was linear. The intercept was very close to zero, indicating Curie behavior. The room temperature magnetic moment was 1.74 μ_B, consistent with one unpaired electron and an *S* value of 1/2. The magnetic susceptibility of the dication (*SS*,*RR*)-$\mathbf{2}^{2+}2PF_6^-$ was similarly checked. The data established an upper limit of 3% of an $S = 1/2$ species, presumably (*SS*,*RR*)-$\mathbf{2}^{\bullet+}PF_6^-$, in the otherwise diamagnetic sample. The temperature dependence of χ_M was inconsistent with a thermally populated triplet excited state.[37a]

Formally, $\mathbf{2}^{\bullet+}PF_6^-$ is a d^6/d^5 or Re(I)/Re(II) mixed valence compound. Many symmetrically substituted d^6/d^5 species have been studied, especially for ruthenium, and can exhibit localized, partially delocalized, or fully delocalized electronic structures (classes I, II, and III).[4] We sought to probe this issue with $\mathbf{2}^{\bullet+}PF_6^-$. First, as summarized in Table 1, IR spectra showed

(34) (a) All K_c values were calculated as follows: $\ln(K_c) = nF(E°_2 - E°_1)/RT = 11604(E°_2 - E°_1)/T$; $\ln(K_c) = 39.25(E°_2 - E°_1)$ at 22.5 °C. These vary appreciably when temperatures are changed by a few degrees, or $E°_2 - E°_1$ values are changed by a few mV. Therefore, only two significant digits are given. Since K_c values are furthermore solvent dependent, literature data should be compared with caution. (b) Values designated by this reference have, for comparative purposes, been recalculated at 22.5 °C as in (a). Consequently, they differ from the original literature report. Also, note that the $E°_2 - E°_1$ values may depend slightly upon temperature.

(35) The decomposed material gave new IR $\upsilon_{C\equiv C}$ bands (cm^{-1}, thin film: 2053 w, 1993 m, 1960 m, 1928 m), a much broader υ_{NO} band (1653 s), an intense new visible absorption (632 nm), and numerous ^1H NMR $C_5(CH_3)_5$ and ^{31}P NMR signals. We speculate that, at least in part, chain−chain coupling occurs to give a diamagnetic, dicationic Re_4C_8 complex consisting of two vinylidene and two alkynyl linkages, and several configurational diastereomers.

(36) Brunner, H.; Fisch, K.; Jones, P. G.; Salbeck, J. *Angew. Chem., Int. Ed. Engl.* **1989**, *28*, 1521.

(37) (a) Miller, J. S.; Dixon, D. A.; Calabrese, J. C.; Vazquez, C.; Krusic, P. J.; Ward, M. D.; Wasserman, E.; Harlow, R. L. *J. Am. Chem. Soc.* **1990**, *112*, 381. (b) Diamagnetic corrections based upon Pascal's constants and measurements with **2** were applied (-833×10^{-6} emu/mol).

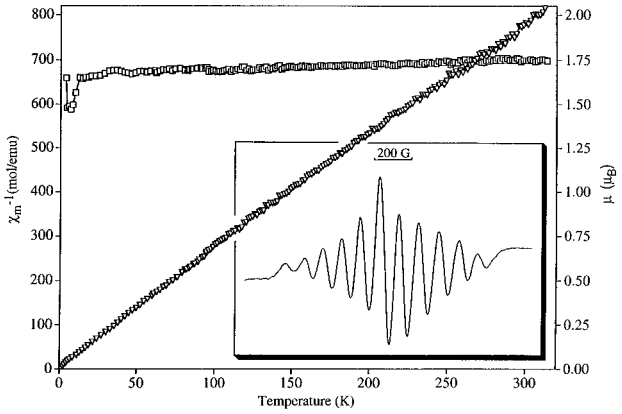

Figure 5. Probes of the paramagnetism of $\mathbf{2}^{\bullet+}PF_6^-$. (a) Temperature dependence of the corrected reciprocal molar magnetic susceptibility, χm^{-1} (▽), and magnetic moment, μ (□). (b) Inset: ESR spectrum of (*SS,RR*)-$\mathbf{2}^{\bullet+}PF_6^-$ (CH_2Cl_2, ambient temperature, 7.0×10^{-3} M).

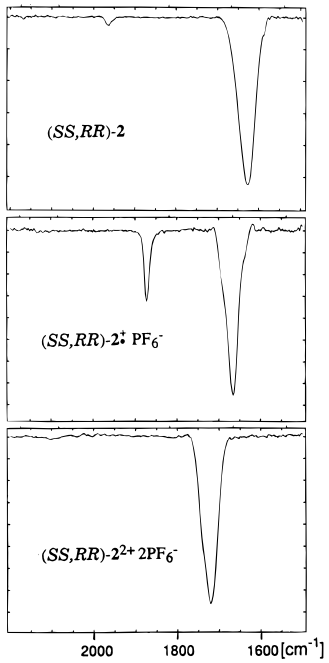

Figure 6. IR ν_{NO} and ν_{CC} absorptions (CH_2Cl_2, ambient temperature, 4-5 $\times 10^{-3}$ M).

a single υ_{NO} band both in solution and the solid state.[24] Second, the band was between those of **2** and $\mathbf{2}^{2+}2PF_6^-$ (Δcm^{-1} 42 and 54, CH_2Cl_2), indicating an intermediate level of backbonding. Third, as illustrated in Figure 6, the half-widths were comparable. If, on the very rapid IR time scale (ca. 10^{-13} s), one rhenium of $\mathbf{2}^{\bullet+}PF_6^-$ were positively charged and the other neutral, two υ_{NO} bands would be expected. Further, IR and Raman spectra each showed a single υ_{CC} band, with frequencies lower than those of **2** (Δcm^{-1} 94−66). The Raman frequency was also higher than that of $\mathbf{2}^{2+}2PF_6^-$ (Δcm^{-1} 107). Hence, we conclude that the ground state of $\mathbf{2}^{\bullet+}PF_6^-$ features a ReC_4Re assembly with bond orders intermediate between those of **2** and $\mathbf{2}^{2+}2PF_6^-$ and a formal half positive charge on each rhenium.

The delocalization of the odd electron in (*SS,RR*)-$\mathbf{2}^{\bullet+}PF_6^-$ was probed by ESR. As depicted in Figure 5 (inset), an undecet (*g* 2.02, CH_2Cl_2) with an $A_{iso,Re}$ value of 98 G and broad individual lines (ΔH_{pp} 49 G) was observed.[24] Rhenium has two principal isotopes with spin 5/2, but since the magnetic moments are very close they can be treated as a single spin system. Thus, the undecet indicates that the two rheniums are equivalent on the rapid ESR time scale (ca. 10^{-9} s). Furthermore, the monorhenium radical cation $[(\eta^5\text{-}C_5Me_5)Re(NO)(PPh_3)(CH_3)]^{\bullet+}PF_6^-$, for which analogous delocalization is impossible, gives a sextet

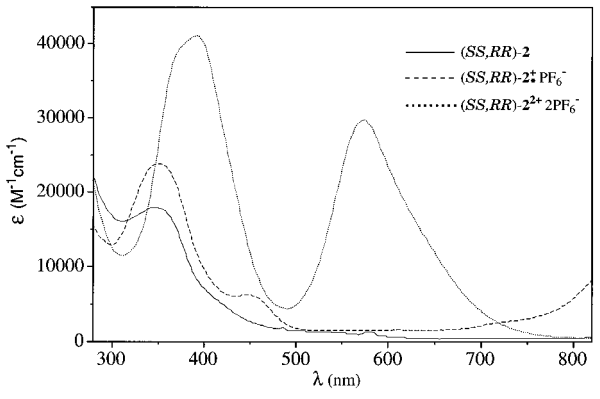

Figure 7. UV/visible spectra of (*SS,RR*)-**2**, (*SS,RR*)-$\mathbf{2}^{\bullet+}PF_6^-$, and (*SS,RR*)-$\mathbf{2}^{2+}2PF_6^-$ (CH_2Cl_2, ambient temperature, $1.7-2.9 \times 10^{-5}$ M).

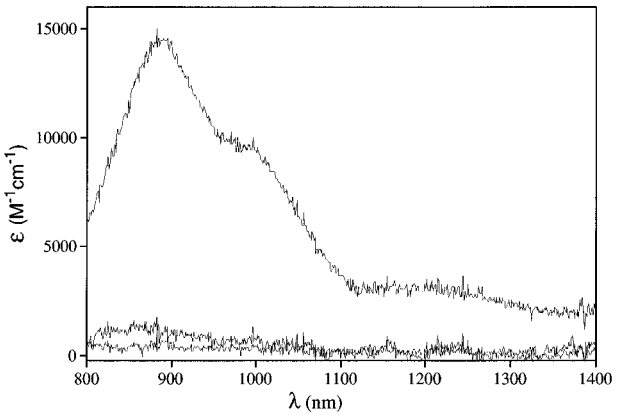

Figure 8. Near-IR spectrum of (*SS,RR*)-$\mathbf{2}^{\bullet+}PF_6^-$ (CH_2Cl_2, ambient temperature, 1.7×10^{-5} M). Background spectra of (*SS,RR*)-**2** and (*SS,RR*)-$\mathbf{2}^{2+}2PF_6^-$ are given for comparison.

with an $A_{iso,Re}$ value that is approximately *twice* as large (195−190 G).[14,38,39] ESR spectra of labeled (*SS,RR*)-$\mathbf{2}^{\bullet+}$-$^{13}C_4PF_6^-$ did not show additional couplings (ΔH_{pp} ca. 45 G). Hence, there is relatively little spin density on the carbon chain, or at phosphorus.

The various classes of mixed valence complexes exhibit distinguishing optical properties.[4,7] Thus, UV/visible/near-IR spectra of $\mathbf{2}^{n+}$ nPF_6^- were recorded under identical conditions in CH_2Cl_2, as illustrated in Figures 7 and 8. Orange-brown (*SS,RR*)-**2** showed an absorption at 350 nm (ϵ 16 900 M^{-1} cm^{-1}) that tailed into the visible.[24] In contrast, the ethynyl complex **1** exhibited only barely discernable shoulders, the most pronounced of which was at 316 nm (ϵ 2300). Deep blue (*SS,RR*)-$\mathbf{2}^{2+}2PF_6^-$ gave two intense bands at 390 and 578 nm (ϵ 39 600, 28 100).[24] Alkylidene and vinylidene complexes of **II**-Me_n with aryl substituents exhibit a single absorption between 360 and 400 nm (ϵ 7600−13 000).[16,27a,b,] These are absent in analogs with alkyl or hydrogen substituents. Hence, the 390 and 578 nm transitions may involve acceptor orbitals with substantial carbon chain character. The former shifted to 368 nm in acetone and 364 nm in CH_3CN, but the latter moved only slightly to 572 nm.[40]

(38) Similar multiplicity and A value relationships have been established for delocalized radical cations with $Mo(PR_3)_2(CO)_3$ termini and pyrazine bridges and radical anions with $Mo(L)_3(NO)(X)$ termini and 1,2- or 1,4-$NH_2C_6H_4NH_2$ bridges: (a) Bruns, W.; Kaim, W.; Waldhör, E.; Krejčik, M. *J. Chem. Soc., Chem. Commun.* **1993**, 1868 and *Inorg. Chem.* **1995**, *34*, 663. (b) Wlodarczyk, A.; Maher, J. P.; McCleverty, J. A.; Ward, M. D. *J. Chem. Soc., Chem. Commun.* **1995**, 2397.

(39) Two isomeric rhenium-centered radicals of the formula $\cdot Re(CO)_3(PCy_3)_2$ give $A_{iso,Re}$ values of 190 and 156 G: Walker, H. W.; Rattinger, G. B.; Belford, R. L.; Brown, T. L. *Organometallics* **1983**, *2*, 775.

Table 4. Near IR Data for $\mathbf{2}^{\bullet+}PF_6^-$ and Quantities Derived Therefrom[a,b]

	band A	band B	band C
λ_{max} or $\tilde{\nu}_{op}$	833/	1000/	1200
(nm/cm^{-1}, CH_2Cl_2)	1132*5*	1000*0*	833*3*
λ_{max} or $\tilde{\nu}_{op}$	885/	997/	1239
(nm/cm^{-1}, acetone)	1129*9*	1003*0*	807*1*
λ_{max} or $\tilde{\nu}_{op}$	884/	1001/	1228
(nm/cm^{-1}, CH_3CN)	1131*2*	999*1*	814*3*
ϵ_{max} (M^{-1} cm^{-1}; CH_2Cl_2)	15*000*	9*400*	3*200*
ϵ_{max} (M^{-1} cm^{-1}; acetone)	15*400*	8*800*	*2600*
ϵ_{max} (M^{-1} cm^{-1}; CH_3CN)	14*900*	8*700*	*3100*
$\Delta\tilde{\nu}_{1/2}$ (cm^{-1}; CH_2Cl_2)[c]	1*800*	1*200*	1*500*
$\Delta\tilde{\nu}_{1/2}$ (cm^{-1}; acetone)[c]	1*800*	1*300*	1*900*
$\Delta\tilde{\nu}_{1/2}$ (cm^{-1}; CH_3CN)[c]	1*800*	1*300*	1*600*
$\tilde{\nu}_{op}$ or $\mathbf{V_{ab}}$, **Class III**	566*3*	500*0*	416*6*
(cm^{-1}/eV)[d]	0.702	0.620	0.51*6*
$(0.0205/r)(\epsilon_{max}\Delta\tilde{\nu}_{1/2}\tilde{\nu}_{op})^{1/2}$	146*6*/	89*0*/	53*0*/
or $\mathbf{V_{ab}}$, **Class II** (cm^{-1}/eV)[d,e]	0.18	0.11	0.07
$(2310\tilde{\nu}_{op})^{1/2}$ or $\Delta\tilde{\nu}_{1/2}$ (calc),	511*5*	480*6*	438*7*
Class II (cm^{-1})[d]			

[a] For general discussions, and additional theoretical background regarding the calculated quantities, see ref 7. [b] Errors in λ_{max} (Figure 8) are estimated as ±3 nm for band A, ±10 nm for band B, and ±30 for band C. These values reflect extensive analyses with curve-fitting programs. Errors in $\Delta\tilde{\nu}_{1/2}$ follow a similar trend. Italicized digits are not significant but were utilized for calculated quantities. [c] $\Delta\tilde{\nu}_{1/2}$ is the full bandwidth at half height. [d] These values are for spectra in CH_2Cl_2. Values in other solvents would be similar. [e] r is the metal−metal distance in Å. The average of the distances in (*SS,RR*)-**2** and (*SS,RR*)-$\mathbf{2}^{2+}2PF_6^-$ was used (7.73 Å).

Deep green (*SS,RR*)-$\mathbf{2}^{\bullet+}PF_6^-$ gave two UV/visible absorptions at 348 and 454 nm (ϵ 24 000, 6400). It also exhibited three near IR bands at 883, 1000 and 1200 nm (ϵ 15 000−3200; Figure 8). Samples enriched in (*SR,RS*)-$\mathbf{2}^{\bullet+}PF_6^-$ gave identical spectra. The near IR absorptions have no counterpart in the other complexes and to facilitate discussion are termed A, B, and C, respectively. Spectra recorded in acetone and CH_3CN were virtually identical, especially considering errors inherent in quantitative analyses of broad, overlapping peaks. Data are summarized in Table 4 and further interpreted below.

6. Computations. We sought to further clarify the electronic and geometrical features of the preceding compounds computationally. Surprisingly, only scant theoretical data for complexes of the type **I** have been reported.[41] To improve tractability, the endgroups **II**-Me_5 were modeled by the smaller isolobal fragment (Cl)Re(NO)(PH_3), and the resulting complexes were distinguished as $\mathbf{2'}^{n+}$. The geometries of the *SS,RR* diastereomers of **2′** and $\mathbf{2'}^{2+}$ were optimized, and the electronic structures were analyzed, using the natural bond orbital (NBO) partitioning scheme developed by Weinhold[42] and the topological analysis of the electron density distribution introduced by Bader.[43] Details are given in the Experimental Section. Unfortunately, computations involving the radical cation $\mathbf{2'}^{\bullet+}$ did not give SCF convergence.

Figure 9 shows the optimized geometries of (*SS,RR*)-**2′** and (*SS,RR*)-$\mathbf{2'}^{2+}$. The calculated bond lengths and angles are in excellent agreement with those in Table 3. Hence, the computational data can confidently be used to analyze bonding and electronic structure of the parent compounds (*SS,RR*)-**2** and (*SS,RR*)-$\mathbf{2}^{2+}2X^-$. For comparative purposes, similar calculations were conducted with butadiyne, the butadiyne dication, and hexapentaene. Key results are also illustrated in Figure 9 and clearly support the μ-butadiynediyl and cumulenic valence formulations given for **2** and $\mathbf{2}^{2+}2PF_6^-$ above.

The change in carbon−carbon bond lengths upon oxidation of butadiyne to the dication (Figure 9) is similar to that for the oxidation of (*SS,RR*)-**2′** to (*SS,RR*)-$\mathbf{2'}^{2+}$. Thus, it might be presumed that the latter involves electron loss from an orbital largely localized on the carbon chain. However, this is not the case. The two highest occupied MOs (57 and 56) are nearly degenerate and have appreciable coefficients on the rhenium and nitrosyl groups as well as some C_4 π character. Accordingly, the structural differences between (*SS,RR*)-**2′** and (*SS,RR*)-$\mathbf{2'}^{2+}$ are not restricted to the carbon chain. As shown in Figure 9, there are sizable changes in the rhenium−ligand bond lengths, most of which are tracked experimentally. The differences in charge distributions are summarized in Table 5. Out of the two electrons removed, 0.74 are lost from the C_4 chain, 0.72 from the nitrosyl ligands, 0.42 from the chlorine ligands, and 0.10 from the PH_3 ligands. Interestingly, the partial charges on rhenium remain nearly the same.

Differences in bond orders are also summarized in Table 5. Upon oxidation, those of the Re−C and ReC***C***−***C*** bonds increase (0.76 to 1.30; 1.14 to 1.76), while that of the Re***C***−***C*** bond decreases (2.67 to 1.95). Topological analysis of the electron density distribution reveals additional electronic structure features. Figure 10 shows contour line diagrams of the Laplacian distribution $\nabla^2\rho(\mathbf{r})$.[44] That of (*SS,RR*)-**2′** in the P−Re−C plane (Figure 10a) clearly shows higher charge concentrations ($\nabla^2\rho(\mathbf{r}) < 0$, solid lines) between the Re***CC*** atoms than the ReC***CC*** atoms. These do not vary as the molecule is rotated about the ReC_4Re axis. In contrast, the Laplacian distribution of (*SS,RR*)-$\mathbf{2'}^{2+}$ shows dramatic differences in this region as the ReC_4Re axis is rotated. This is illustrated in Figure 10b for the P−Re−C plane, and Figure 10c for an orthogonal plane. The charge concentration is smaller between the Re***CC*** atoms than the ReC***CC*** atoms in the former and reversed in the latter.[44] This anisotropy, and all of the preceding data, provide overwhelming support for a cumulenic valence formulation for $\mathbf{2}^{2+}2PF_6^-$.

The geometries of (*SS,RR*)-**2′** and (*SS,RR*)-$\mathbf{2'}^{2+}$ were optimized without any symmetry constraints, except that the phosphorus−hydrogen distances were forced to be the same. In the former, the P−Re−C planes define a smaller angle (106.5°; Figure 9) than in (*SS,RR*)-**2** (148.4°; Figure 3, Table 3). This is likely a simple steric consequence of the bulkier phosphine in **2**. Accordingly, there is little change in computed bond lengths as the rhenium termini are rotated. The P−Re−C planes in (*SS,RR*)-$\mathbf{2'}^{2+}$ define a 168.9° angle, giving an anti orientation of PH_3 ligands. This corresponds to geometric isomer **V** in Scheme 3, supporting the stability order assigned above (**V** > **VI**). Finally, the alternating sp/sp C═C bond lengths in (*SS,RR*)-$\mathbf{2}^{2+}2PF_6^-$ and a hexapentaene (Figure 4, bottom) are also reproduced theoretically. This possibly general feature of certain higher cumulenes appears to have received little attention.[32b,45] As a simple and intuitive rationale, consider

(40) For comparison, the benzylidene complex[27b] [(η^5-C_5H_5)Re(NO)-(PPh_3)(═CHPh)]$^+PF_6^-$ was also checked for solvatochromism: CH_2Cl_2, 368 nm; acetone, 366 nm; CH_3CN, 366 nm (ϵ 14 900, 12 900, 13 200 M^{-1} cm^{-1}).

(41) (a) Frapper, G.; Kertesz, M. *Inorg. Chem.* **1993**, *32*, 732. (b) Sponsler, M. B. *Organometallics* **1995**, *14*, 1920. (c) Belanzoni, P.; Re, N.; Rosi, M.; Sgamellotti, A.; Floriani, C. *Organometallics* **1996**, *15*, 4264

(42) Reed, A. E.; Curtiss, L. A.; Weinhold, F. *Chem. Rev.* **1988**, *88*, 899.

(43) Bader, R. F. W. *Atoms in Molecules: A Quantum Theory*; Oxford University Press: New York, 1990.

(44) (a) Note that $\nabla^2\rho(\mathbf{r})$ is the second derivative of the electron density $\rho(\mathbf{r})$. A function is said to be concentrated in a region where its second derivative is negative. One way of comparing Figure 10a−c involves the tightly spaced solid contour lines that encircle C1−C4. These extend further from the atoms about π bonds (e.g., C1−C2 vs C2−C3 in Figure 10a). (b) For quantitative comparisons, the values of the Laplacian at the bond critical points can used. These are −30.606 and −24.525 eÅ^{-5} for the Re***CC*** and ReC***CC*** bonds of (*SS,RR*)-**2′**, and −32.799 and −30.069 eÅ^{-5} for (*SS,RR*)-$\mathbf{2'}^{2+}$. The corresponding electron densities are 2.793, 2.128, 2.585, and 2.499 eÅ^{-3}.

(45) Liang, C.; Allen, L. C. *J. Am. Chem. Soc.* **1991**, *113*, 1873.

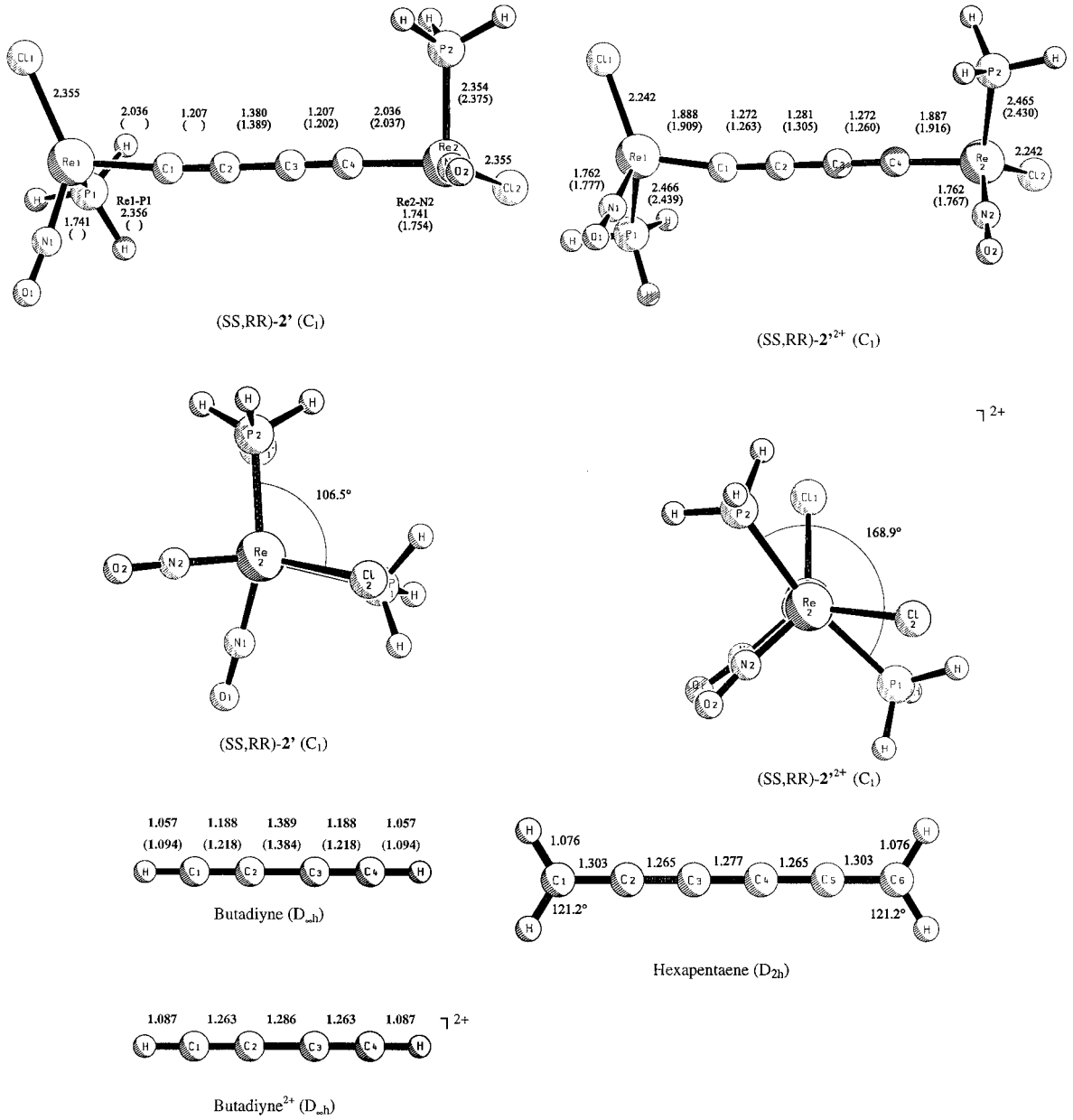

Figure 9. Optimized geometries at HF/II of (*SS,RR*)-**2′** (*SS,RR*)-**2′**$^{2+}$, butadiyne, butadiyne^{2+}, and hexapentaene. Selected experimental values for (*SS,RR*)-**2** and (*SS,RR*)-**2**$^{2+}$2PF_6^- are given in parentheses.

Table 5. Calculated NBO Charge Distribution and Bond Orders of (*SS,RR*)-**2′** and (*SS,RR*)-**2′**$^{2+}$

	(*SS,RR*)-**2′**	(*SS,RR*)-**2′**$^{2+}$	Δ((*SS,RR*)-**2′**$^{2+}$-(*SS,RR*)-**2′**)
		Charges	
Re1	+0.83	+0.81	−0.02
Re2	+0.83	+0.81	−0.02
Re***C***	−0.37	−0.08	+0.58[a]
ReC***C***	−0.13	−0.05	+0.16[a]
∑CCCC	−1.00	−0.26	+0.74
NO	−0.20	+0.16	+0.72[a]
PH_3	+0.46	+0.51	+0.10[a]
Cl	−0.57	−0.36	+0.42[a]
		Bond Orders	
Re−C	0.76	1.30	+0.54
Re−N	1.60	1.43	−0.17
Re−Cl	0.56	0.77	+0.21
Re−P	0.76	0.68	−0.08
Re***C***−***C***	2.67	1.95	−0.72
ReC***C***−***C***	1.14	1.76	+0.62

[a] Difference for two groups.

all zwitterionic and biradical resonance forms of $R_2C{=}(C{=}C)_n{=}CR_2$ in which one charge or unpaired electron is maintained on a sp^2 terminus. These entail various combinations of decreases in the bond orders of $R_2C{=}C$ and $R_2(CC)_xC{=}C$ linkages and increases in bond orders of $R_2CC{=}C$ and $R_2C(CC)_xC{=}C$ linkages.

Discussion

1. Synthetic Methodology. There are now sufficient numbers of complexes **I** with higher carbon chains to allow generalizations regarding synthetic strategies. First, the oxidative coupling of terminal alkynes with $Cu(OAc)_2$/pyridine as in Scheme 2 is commonly referred to as the Eglinton reaction.[22] Previously, this procedure has rarely been applied in a metal coordination sphere.[46] However, it has now been extended to (1) higher homologs of ethynyl complex **1**, affording analogous C_8, C_{12}, C_{16}, and C_{20} complexes,[13a,b] (2) ethynyl and butadiynyl complexes of other metal fragments, giving the corresponding C_4 and C_8 complexes,[18,19c,20h] and (3) cross couplings of ethynyl

(46) Prior examples: (a) For ferrocene derivatives, see Schlögl, K.; Steyrer, W. *J. Organomet. Chem.* **1966**, *6*, 399. (b) Diederich, F.; Rubin, Y.; Chapman, O. L.; Goroff, N. S. *Helv. Chim. Acta* **1994**, *77*, 1441, and earlier references therein.

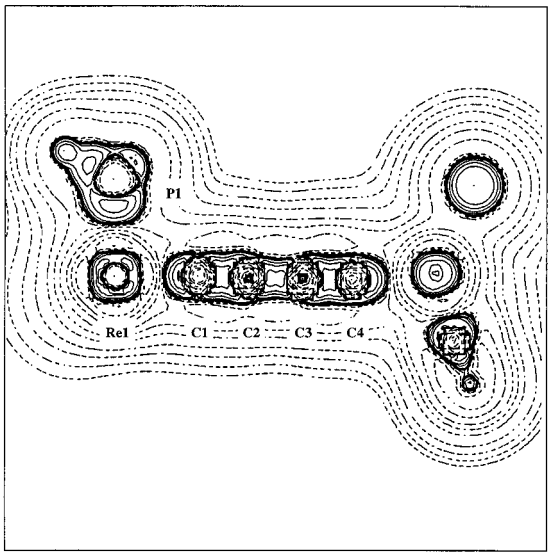

(a) (SS,RR)-**2'**

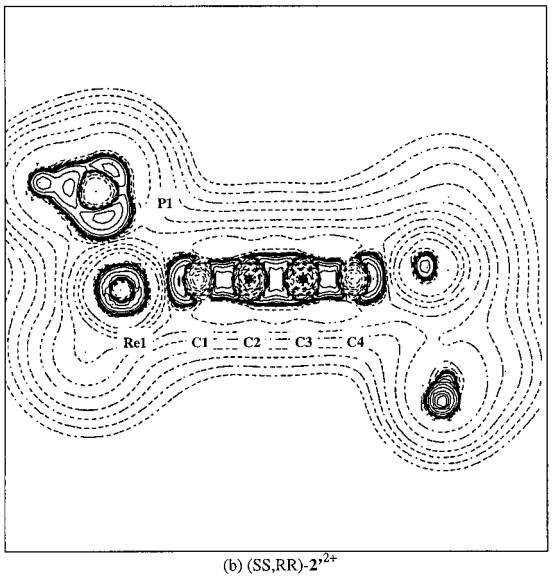

(b) (SS,RR)-$\mathbf{2'}^{2+}$

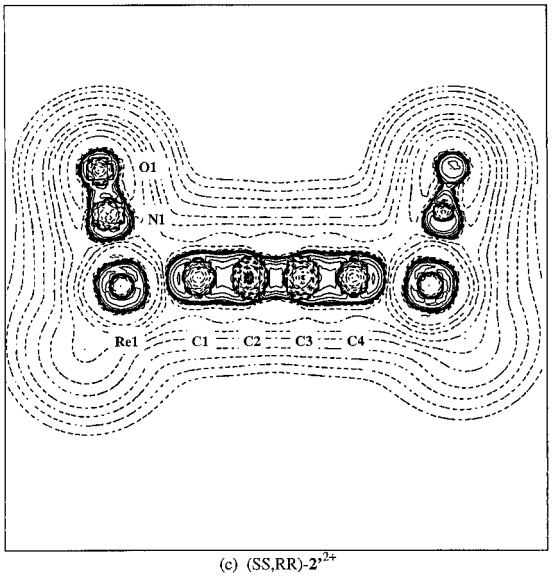

(c) (SS,RR)-$\mathbf{2'}^{2+}$

Figure 10. Contour line diagrams of the Laplacian distribution $\nabla^2\rho(\mathbf{r})$ of (a) (*SS,RR*)-**2′** in the P−Re−C plane; (b) (*SS,RR*)-$\mathbf{2}^{2+}$ in the P−Re−C plane; (c) (*SS,RR*)-$\mathbf{2'}^{2+}$ in a plane orthogonal to that in (b). Dashed lines indicate charge depletion ($\nabla^2\rho(\mathbf{r}) > 0$), and solid lines indicate charge concentration ($\nabla^2\rho(\mathbf{r}) < 0$).[44]

Scheme 5. Other Consanguineous Families of Coordinated Carbon

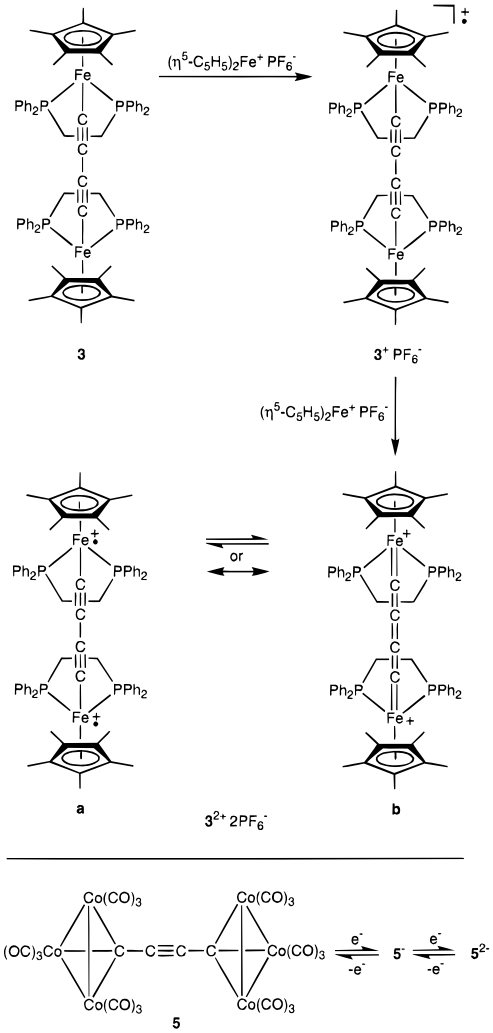

and butadiynyl complexes to C_6 complexes.[13a,18] There is an early report of symmetrical couplings of ethynyl and butadiynyl complexes with O_2 and a CuCl catalyst (Glaser reaction).[47] However, the resulting C_4 and C_8 complexes were only partially characterized. This recipe has also been used to prepare a polymer with a PtC_8Pt repeat unit[48] but is much less effective than the Eglinton conditions with **1**.

As noted above, Lapinte has isolated a series of FeC_4Fe complexes that are closely related to $\mathbf{2}^{n+}$ nPF_6^-: (η^5-C_5Me_5)-Fe(dppe)(C≡CC≡C)(dppe)Fe(η^5-C_5Me_5) (**3**), $\mathbf{3}^{\bullet+}PF_6^-$, and $\mathbf{3}^{2+}2PF_6^-$.[19a,b] These are illustrated in Scheme 5 and discussed in detail below. They are accessed via a one electron oxidation of the iron ethynyl complex (η^5-C_5Me_5)Fe(dppe)(C≡CH). The resulting radical cation dimerizes to give a diiron dication with a divinylidene (=C=CH-HC=C=) bridge, which is then deprotonated to give **3**. All other routes to C_4 complexes reported to date utilize preformed C_4 building blocks, to which the metal termini are attached either in discrete steps[20a,b] or in unison.[20c−g,i,j] Also, all C_4 complexes except those derived from the oxidation of **2** and **3** have μ-butadiynediyl bridges.

Thus, $\mathbf{2}^{n+}$ nPF_6^- and $\mathbf{3}^{n+}$ nPF_6^- presently constitute the only C_4 complexes that have been isolated in more than one redox state. Since electrons are appropriately regarded as the "lifeblood" of molecules, we refer to such families as

(47) Kim, P. J.; Masai, H.; Sonogashira, K.; Hagihara, N. *Inorg. Nucl. Chem. Lett.* **1970**, *6*, 181.

(48) Takahashi, S.; Murata, E.; Sonogashira, K.; Hagihara, N. *J. Poly. Sci.* **1980**, *18*, 661.

consanguineous—in other words, derived from a common ancestor and differing only in electron count.[49] Surprisingly, no consanguineous C_2 complexes have been isolated to date. However, we have prepared compounds with ReC≡CPd and ReC≡CC≡CPdC≡CC≡CRe linkages and characterized the corresponding radical cations in solution.[14] Furthermore, Lapinte has isolated the C_8 homologs of **3** and $\mathbf{3}^{\bullet+}PF_6^-$.[19c]

An obvious potential improvement in our methodology deserves comment. Many complexes of **II**-Me_5 are available in enantiomerically pure form. These would in principle allow the selective preparation of the non-*meso*, enantiomerically pure *SS* or *RR* diastereomers of **2**. However, the immediate precursor to **1**, a cationic π ethyne complex, has to date only been accessed in 90% ee.[50] Furthermore, adducts of **II**-Me_5 tend to be configurationally less stable than cyclopentadienyl analogs, and nonracemic complexes are almost always less crystalline. Accordingly, attempts to prepare diastereomerically pure **2** or higher homologs by this strategy have been disappointing and hampered by a lack of enantiomer purity assays at key stages.[51] Curiously, Eglinton couplings in the cyclopentadienyl series have been unsuccessful, thereby blocking a diastereoselective entry into a related class of compounds.

2. Electronic Structure. The ground state electronic structures of dirhenium complexes $\mathbf{2}^{n+}$ nPF_6^- deserve close scrutiny. First, the μ-butadiynediyl valence formulation of **2** is supported by an overwhelming amount of structural, spectroscopic, and computational data. However, higher homologs will have increasing numbers of resonance forms with reduced C≡C bond orders and increased C−C bond orders. Thus, there is the possibility of a gradual, asymptotic approach to a median or limiting bond length. Hints of such trends can be discerned in a recent review of structurally characterized 1,3,5,7-tetraynes.[13c] Furthermore, there may be attendant effects upon reactivity, as the C_{20} homolog of **2** is considerably more labile.[13b]

The μ-butatrienediylidene or cumulenic valence formulation of $\mathbf{2}^{2+}2PF_6^-$ is supported by (1) the experimental bond lengths (Table 3), (2) the existence of geometric isomers about the ReC_4-Re linkage (Scheme 3), (3) the contrasteric *syn* orientation of PPh_3 ligands in the crystal structure (Figure 4), (4) the Raman υ_{CC} value (Table 1), (5) the $^1J_{CC}$ values,[23] (6) the lack of a magnetic moment, (7) the calculated bond lengths and orders (Figure 9, Table 5), and (8) the change in the Laplacian distribution as the ReC_4Re axis is rotated (Figure 10b,c). This detailed breakdown is prompted by several observations. First, Lapinte's diiron complex $\mathbf{3}^{2+}$ $2PF_6^-$ exhibits contrasting properties, as described below. Second, the geometric isomers of $\mathbf{2}^{2+}2PF_6^-$ interconvert with barriers lower than those of similar alkylidene or vinylidene complexes (11.6−13.5 vs 18−21 kcal/mol),[16,17,26,27] suggesting weaker Re=C bonds and less effective electronic coupling. Third, as noted above, the sp/sp C=C bond length patterns in Figure 4 can be interpreted in terms of increasing contributions by resonance forms with C≡C and C−C linkages. Thus, there is a distinct possibility that immediately higher homologs may have paramagnetic, triplet biradical ground states ($S = 1$) best described by the valence formulation $^{+\bullet}$ReC≡C(C≡C)$_x$C≡CRe$^{\bullet+}$.

With the radical cation $\mathbf{2}^{\bullet+}PF_6^-$, IR and ESR data unambiguously show that the rhenium termini are equivalent on the very

Scheme 6. Other Resonance and Equilibrium Relationships

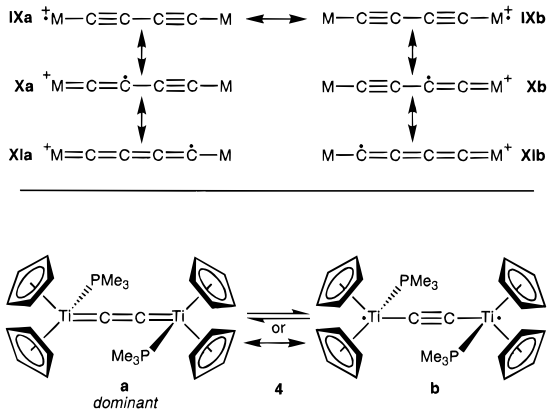

rapid time scales associated with these probes (ca. 10^{-13}, 10^{-9} s). Accordingly, the ground state can be viewed as a resonance hybrid of structures **IX**−**XI** in Scheme 6 (M = Re), such that there is a formal half positive charge on each rhenium, and the odd electron is completely delocalized across the wire-like bridge. Of these, the ESR data indicate that the two with spin density on rhenium, $^{+\bullet}$ReC≡CC≡CRe and ReC≡CC≡CRe$^{\bullet+}$ (**IXa**,**b**), dominate. Analogous electronic structures have been established for other mixed valence compounds with unsaturated bridging ligands. As noted above, these are commonly termed "class III".[4,7]

Most mixed valence compounds exhibit a near IR band, and these also can be used to probe the electronic ground state.[4,7] With class III complexes, the absorptions derive from $\pi \rightarrow \pi^*$ transitions. With localized (class I) or partially delocalized (class II) complexes, they arise from intervalence or metal-to-metal charge transfer (IVCT). Since IVCT transitions entail large changes in charge distributions, often over considerable distances, they usually show marked solvent dependences. Importantly, $\mathbf{2}^{\bullet+}PF_6^-$ gives, within measurement error, solvent independent bands (Figure 8 and Table 4), consistent with the class III assignment. However, $\mathbf{2}^{\bullet+}PF_6^-$ also exhibits three bands, whereas most mixed valence complexes give only one band. Thus, possible rationales were considered.

First, near IR bands are not uncommon in radicals.[52] For example, the conjugated radical cations $[R(CH{=}CH)_nR]^{\bullet+}$ (n = 3−13), which can be viewed as oxidized oligomers of polyacetylene, give progressively red-shifted absorptions.[52a] Also, the monochromium radical (η^5-C_5Ph_5)$Cr(CO)_3^{\bullet}$ exhibits a very broad band near 2500 nm.[52b] Second, spin-orbit coupling is much more pronounced with third-row transition metals and can lift degeneracies in optical transitions. Accordingly, class I, II, and III diosmium and osmium/ruthenium mixed valence complexes exhibit two to three near IR bands.[53] We believe this to be the most likely explanation for the multiple absorptions in Figure 8.

The near IR bands of mixed valence compounds can furthermore be used to calculate electronic coupling parameters V_{ab} (also denoted by other symbols).[7] With class III complexes, V_{ab} can be viewed as a resonance stabilization energy, and the simple formula in Table 4 is applied. Unfortunately, standard protocols have not been developed for compounds that exhibit multiple absorptions due to spin-orbit coupling. Depending

(49) Such sociology-based terminology could be useful in distinguishing other classes of C_x complexes **I**. For example, *conjugal* families would feature two unlike metal fragments. Many believe that there is a need for more humanistic metaphors, and fewer militaristic metaphors, in the chemical literature.

(50) Peng, T.-S.; Winter, C. H.; Gladysz, J. A. *Inorg. Chem.* **1994**, *33*, 2534.

(51) A sample of the cationic π ethyne complex that was a 95:5 enantiomer mixture has been converted to **2** that was a 71:29 diastereomer mixture: Bartik, B., unpublished results, 1994.

(52) (a) Bally, T.; Roth, K.; Tang, W.; Schrock, R. R.; Knoll, K.; Park, L. Y. *J. Am. Chem. Soc.* **1992**, *114*, 2440. (b) Atwood, C. G.; Geiger, W. E. *J. Am. Chem. Soc.* **1994**, *116*, 10849.

(53) (a) Kober, E. M.; Goldsby, K. A.; Narayane, D. N. S.; Meyer, T. J. *J. Am. Chem. Soc.* **1983**, *105*, 4303, and references therein. (b) Lay, P. A.; Magnuson, R. H.; Taube, H. *Inorg. Chem.* **1988**, *27*, 2364. (c) Laidlaw, W. M.; Denning, R. G. *J. Chem. Soc., Dalton Trans.* **1995**, 1987 and references therein.

upon the band of $\mathbf{2}^{\bullet+}PF_6^-$ used, values of 5663−4166 cm^{-1} or 0.702−0.516 eV are obtained (Table 4). In other cases where spectroscopic degeneracies are lifted, the most physically meaningful parameters are usually extracted from the middle absorption, or the most intense absorption. Thus, we suggest that the values associated with band C can be disregarded in comparisons with other compounds (below).

A final point concerns another common test for class III complexes. This entails calculating the band widths $\tilde{\nu}_{1/2}$ according to the formula for class II systems at the bottom of Table 4.[4] In all cases, the resulting values (5115−4387 cm^{-1}) are two to three times greater than those observed (1800−1200 cm^{-1}). Hence, in accord with the above conclusions, $\mathbf{2}^{\bullet+}PF_6^-$ fails what is often regarded as a diagnostic criterion for class II complexes.[54] Nonetheless, to facilitate comparisons with other literature treatments, V_{ab} values are also calculated using the class II formula given in Table 4.

3. Comparisons to Other Complexes. The abundance of data for our dirhenium complexes $\mathbf{2}^{n+}$ nPF_6^- and Lapinte's diiron complexes[19a,b] $\mathbf{3}^{n+}$ nPF_6^- enable a variety of interesting comparisons. First, the crystal structures available to date are complementary: (*SS*,*RR*)-**2** and (*SS*,*RR*)-$\mathbf{2}^{2+}2PF_6^-$ in one series and $\mathbf{3}^{\bullet+}PF_6^-$ in the other. The metal−metal distance in the latter is shorter than in either dirhenium complex (7.431(2) vs 7.8288(4)-7.6350(8) Å), as would be expected from the intrinsic contraction in iron−ligand bond lengths. The degree of chain bending (∠C−C−Fe/C, 167.0(6)°/177(1)°) is similar to that of (*SS*,*RR*)-$\mathbf{2}^{2+}2PF_6^-$, whereas the carbon−carbon bond lengths (1.236 (9), 1.36(1) Å) are closer to those in (*SS*,*RR*)-**2**. Also, the second tertiary phosphine moiety renders the iron endgroups bulkier. Thus, **3** gives a detectable barrier to rotation about the MC_4M linkage ($\Delta G^{\ddagger}$(220 K) = 9.9 kcal/mol), but not **2** (−110 °C, THF; −80 °C, CD_2Cl_2). Of course, the greater metal−metal distance in **2** may also be a contributing factor.

The second tertiary phosphine also renders the iron endgroups more electron releasing. Thus, the $E°$ values, which were measured by cyclic voltammetry under identical conditions in CH_2Cl_2, show that the diiron complexes are much easier to oxidize thermodynamically ($E°_1/E°_2$: −0.675/0.045 vs 0.01/0.54 V).[25] Furthermore, the $E°_1$ and $E°_2$ values differ more in the diiron series, giving a larger equilibrium constant for comproportionation (K_c 1.9 × 10^{12} (22.5 °C)[34b] vs 1.1 × 10^9 (22.5 °C)). Note that the greater the (1) resonance stabilization of the mixed valence species or (2) electrostatic repulsion associated with the second positive charge, the more facile the first oxidation relative to the second. Thus, K_c values provide an alternative measure of electronic coupling between metal centers and usually track V_{ab} values. However, there can be substantial solvent dependences, as exemplified by the >50 fold decrease in K_c for the dirhenium complexes in the more polar solvent CH_3CN (2.1 × 10^7).

The ground state electronic structures of **2** and **3** are analogous. However, $\mathbf{3}^{2+}$ $2PF_6^-$ exhibits ^1H NMR signals over a much wider chemical shift range (δ −7 to 10) than $\mathbf{2}^{2+}2PF_6^-$. Also, the IR υ_{CC} bands (2160 w, 1950 m; cm^{-1}, CH_2Cl_2) are at *higher* frequency than those of $\mathbf{3}^{\bullet+}PF_6^-$ (1973 w, 1880 m) or **3** (1955 m, 1880 w). The IR/Raman trend is opposite in the dirhenium series (Table 1), paralleling the bond orders. Furthermore, $\mathbf{3}^{2+}$ $2PF_6^-$ gives magnetic moments of 1.29 and 1.37 μ_B in solution and the solid state. Although no ESR signal can be detected, paramagnetic compounds are often ESR silent. Thus, $\mathbf{3}^{2+}$ $2PF_6^-$ may have a triplet biradical ground state (S = 1) that is best described by a $^{+\bullet}FeC{\equiv}CC{\equiv}CFe^{\bullet+}$ valence formulation as shown in $\mathbf{3a}^{\bullet+}PF_6^-$ in Scheme 5. Alternatively, these data may reflect a much lower singlet/triplet energy spacing than for $\mathbf{2}^{2+}2PF_6^-$. Regardless, there appears to be either a stronger electronic coupling of metal centers with rhenium or a greater stabilization of an open shell structure with iron.

The radical cations $\mathbf{2}^{\bullet+}PF_6^-$ and $\mathbf{3}^{\bullet+}PF_6^-$ both have delocalized ground state electronic structures, as represented in Scheme 6 (top). Importantly, this conclusion is reinforced by complementary arrays of spectroscopic tests. For example, the iron termini in $\mathbf{3}^{\bullet+}PF_6^-$ can be uniquely probed by Mössbauer spectroscopy. Only one doublet is observed at temperatures as low as 4.2 K, with a quadrupole splitting close to the average of **3** and $\mathbf{3}^{2+}$ $2PF_6^-$. Thus, only one type of iron is present on the rapid time scale of this measurement (10^{-9} s). Similarly, the PF_6^- anion is symmetrically disposed with regard to the iron termini in crystalline $\mathbf{3}^{\bullet+}PF_6^-$. As detailed above, the dirhenium analog $\mathbf{2}^{\bullet+}PF_6^-$ offers a nitrosyl spectator ligand with an intense IR absorption that is very sensitive to charge, as well as easily interpreted ESR multiplicity and $A_{iso,Re}$ values.

In contrast to $\mathbf{2}^{\bullet+}PF_6^-$, $\mathbf{3}^{\bullet+}PF_6^-$ gives a single near IR band, which is as expected solvent independent. Therefore, V_{ab} can be unambiguously calculated. Using the class III formula (Table 4), a value of 0.47 eV is obtained, as compared to 0.702 eV from the most intense band A of $\mathbf{2}^{\bullet+}PF_6^-$, or 0.620 eV from the "average" band B. A slightly inverted trend is obtained from the class II formula (0.19 eV vs 0.18 or 0.11 eV). In view of the approximations inherent in these treatments, we hesitate to infer that there is stronger electronic coupling in $\mathbf{2}^{\bullet+}PF_6^-$, particularly in view of the lower K_c value. However, it is clear that both ours and Lapinte's mixed valence complexes rank with the most strongly coupled in the literature, regardless of spacer type or metal−metal distance.[55]

Additional comparisons are possible with other complexes of the type **I**. For example, the issue of diamagnetic, singlet vs paramagnetic, triplet electronic ground states has been probed at least once previously.[56] As shown in Scheme 6 (bottom), the dititanium C_2 complex (η^5-C_5H_5)$_2$Ti(PMe_3)(CC)(Me_3P)Ti(η^5-C_5H_5)$_2$ (**4**) can be plausibly formulated with either Ti═C═C═Ti or $^{\bullet}$Ti-C≡C-Ti$^{\bullet}$ linkages. The former (**4a**) is characterized by Ti(IV) or Ti(II) termini, whereas the latter (**4b**) has Ti(III) termini. All possibilities have abundant precedent in bis(cyclopentadienyl) titanium compounds. The NMR and crystallographic data clearly established the spin-paired ground state **4a**.

As shown in Scheme 5, the carbon termini of the hexacobalt C_4 complex $(CO)_9Co_3CC{\equiv}CCCo_3(CO)_9$ (**5**)[57] are bound to *three* metals, as opposed to a single metal as in **I**. Hence, this represents a different class of carbon chain complex, although the valence situation is reminiscent of that in **Ic** (Scheme 1). Regardless, **5** undergoes two chemically reversible one electron reductions with $E°_1$ and $E°_2$ values that differ by 0.20−0.30 V, depending upon solvent. This hints at another potentially

(54) For a caveat, see: Atwood, C. G.; Geiger, W. E.; Rheingold, A. L. *J. Am. Chem. Soc.* **1993**, *115*, 5310.

(55) Additional symmetrical class III complexes with high V_{ab} or K_c values can be located through ref 3, 7, 19, 38, 40b, 50b, and the following. (a) V_{ab} 5320 cm^{-1}, K_c 3.3 × 10^8 (CH_3CN, 22.5 °C):[34b] Spreer, L. O.; Li, A.; MacQueen, D. B.; Allan, C. B.; Otvos, J. W.; Calvin, M.; Frankel, R. B.; Papaefthymious, G. C. *Inorg. Chem.* **1994**, *33*, 1753. (b) V_{ab} 6200 cm^{-1}, K_c 4.8 × 10^{15} (CH_3CN, 22.5 °C):[34b] Spreer, L. O.; Allan, C. B.; MacQueen, D. B.; Otvos, J. W.; Calvin, M. *J. Am. Chem. Soc.* **1994**, *116*, 2187. (c) K_c 3.6 × 10^{17} (THF, 22.5 °C):[34b] Manriquez, J. M.; Ward, M. D.; Reiff, W. M.; Calabrese, J. C.; Jones, N. L.; Carroll, P. J.; Bunel, E. E.; Miller, J. S. *J. Am. Chem. Soc.* **1995**, *117*, 6182. (d) V_{ab} 2800 cm^{-1}, K_c 5.2 × 10^9 (CH_3CN, 22.5 °C):[34b] Bardwell, D. A.; Horsburgh, L.; Jeffery, J. C.; Joulié, L. F.; Ward, M. D.; Webster, I.; Yellowlees, L. J. *J. Chem. Soc., Dalton Trans.* **1996**, 2527.

(56) Binger, P.; Müller, P.; Phillips, P.; Gabor, B.; Mynott, R.; Herrmann, A. T.; Langhauser, F.; Krüger, C. *Chem. Ber.* **1992**, *125*, 2209.

(57) (a) Worth, G. H.; Robinson, B. H.; Simpson, J. *Organometallics* **1992**, *11*, 3863. (b) Osella, D.; Gambino, O.; Nevi, C.; Ravera, M.; Bertolino, D. *Inorg. Chim. Acta* **1993**, *206*, 155.

isolable consanguineous family. Finally, cyclic voltammograms of the dirhenium C_4 complex (*t*-Bu_2bpy)$(CO)_3$Re(C≡CC≡C)-Re$(CO)_3$(*t*-Bu_2bpy) show only irreversible oxidations and reductions.[20h]

4. Longer Carbon Chains. The unsaturated ReC_4Re linkage in $\mathbf{2}^{\bullet+}PF_6^-$ allows electron delocalization over a six atom, 7.73 Å span. The most compelling question, from a variety of theoretical and practical standpoints, concerns the behavior of higher and more wire-like homologs. This in turn interfaces with the topical subject of carbon allotropes.[9] Importantly, the classical polymeric sp^3 and sp^2 allotropes, diamond and graphite, must terminate with endgroups that differ from their repeat units. Thus, at sufficiently high chain lengths, C_x complexes **I** can analogously be viewed as polymeric sp carbon allotropes.

Indeed, the carbon chains in $\mathbf{2}^{n+}$ nPF_6^- can be significantly extended. The longest chain complex isolated to date is the C_{20} homolog of **2**, which features ten conjugated triple bonds.[13b] However, the polyalkynyl compounds exhibit progressively less reversible oxidations and diminishing $E°_2-E°_1$ values (0.28, 0.19, 0.09, and 0.00 V (CH_2Cl_2) for C_8, C_{12}, C_{16}, and C_{20} chains). The latter translate into decreasing K_c values (5.9×10^4, 1.7×10^3, 3.4×10^1, 4; 22.5 °C) and degrees of electronic coupling between the termini. Analogous trends have been observed for bimetallic complexes in which pyridyl or cyclopentadienyl ligands are linked by polyalk*enyl* bridges.[3,58] The K_c value of the C_8 homolog of $\mathbf{3}^{\bullet+}PF_6^-$ drops by a similar order of magnitude (2.1×10^7 vs 1.9×10^{12}, 22.5 °C),[34b] although the V_{ab} value remains comparable (0.32 vs 0.47 eV).[19c]

We have begun to explore strategies that may increase electronic communication between rhenium termini. In one effort, similar complexes with ReC≡CC≡CPdC≡CC≡CRe linkages have been studied.[14] However, oxidation gives a radical cation that, on the ESR time scale, remains localized on one rhenium (sextet, $A_{iso,Re} = 140$ G). Hence, the palladium does not provide an efficient "relay". Another effort involves analogs of $\mathbf{2}^{n+}$ nPF_6^- with more electron releasing and bulkier phosphines.[18] More electron releasing spectator ligands should facilitate oxidation and have the potential to increase electronic coupling. Indeed, slightly higher V_{ab} and K_c values have been obtained.[18] Bulkier spectator ligands may retard the dimerization that is suspected as the major decomposition pathway for the radical cations.[35]

Finally, there are many other attractive directions in which the present body of data can be extended. As noted above, *conjugal* families of C_x complexes with iron and rhenium endgroups are now available[21] and will provide additional insight regarding many of the questions involving $\mathbf{2}^{n+}$ nPF_6^- and $\mathbf{3}^{n+}$ nPF_6^-. Furthermore, alkynyl and polyalkynyl linkages are of exceptional utility in a variety of materials chemistry applications, featuring prominently in macrocycles, porphyrin arrays, rigid rod polymers, sensory materials, and liquid crystals.[59] Numerous supramolecular assemblies are also readily envisioned. These and other themes will be represented in future reports from this laboratory.

Experimental Section

General Data. Most instruments and general procedures have been described previously.[14,37] Near IR spectra were recorded on a CARY 17 spectrometer. Solvents were purified as follows: CH_2Cl_2/CD_2Cl_2, distilled/vacuum transferred from CaH_2; ether, THF, hexane, benzene, distilled from Na/benzophenone; toluene, distilled from Na; C_6D_6, vacuum transferred from $LiAlH_4$. Other materials were used as received.

(η^5-C_5Me_5)Re(NO)(PPh$_3$)(C≡CC≡C)(Ph$_3$P)(ON)Re(η^5-C_5Me_5) (2). A Schlenk tube was charged with (η^5-C_5Me_5)Re(NO)(PPh_3)(C≡CH) (**1**, 0.200 g, 0.313 mmol),[17] $Cu(OAc)_2$ (0.085 g, 0.47 mmol) and pyridine (3 mL). The mixture was stirred for 2 h at 80 °C (oil bath). Solvent was removed by mechanical oil pump vacuum, and the residue was dissolved in THF (5 mL). Silica gel column chromatography (THF) gave an orange-red fraction. Solvent was removed by oil pump vacuum to give **2** as an orange-brown powder (0.176 g, 0.138 mmol, 88%).

(*SS,RR*)-2·2CH$_2$Cl$_2$. The preceding sample of **2** was dissolved in a minimum of CH_2Cl_2. A layer of hexane was gently added. After 24 h, the red-orange microcrystals were collected by filtration and dried by oil pump vacuum to give (*SS,RR*)-**2**·$2CH_2Cl_2$ (0.040 g, 0.028 mmol, 20%), mp > 250 °C. Calcd for $C_{62}H_{64}Cl_4N_2O_2P_2Re_2$: C, 51.52; H, 4.46; Cl, 9.81. Found: C, 51.69; H, 4.50; Cl, 9.59. IR/Raman, Table 1; ^{1}H NMR (δ, THF-d_8) 7.56−7.48 (m, 12H of $6C_6H_5$), 7.26−7.17 (m, 18H of $6C_6H_5$), 1.68 (s, $2C_5(CH_3)_5$); ^{13}C{^{1}H} NMR (ppm, THF-d_8) 135.2 (s, *o*-Ph), 130.3 (s, *p*-Ph), 128.5 (s, *m*-Ph), 100.71 (s, ***C***$_5$-$(CH_3)_5$), 10.28 (s, C_5(***C***$H_3)_5$); ^{31}P{^{1}H} NMR (ppm, THF-d_8) 21.8 (br s); UV/vis (nm (ϵ, M^{-1} cm^{-1}), 1.7×10^{-5} M CH_2Cl_2) 232 (65 000), 270 sh (31 000), 346 (20 500); MS (positive FAB, 3-NBA/benzene)[60] 1276 (**2**$^+$, 100%), 614 ((η^5-C_5Me_5)Re(NO)(PPh_3)$^+$, 89%); no other peaks above 310 of >45%.

(*SR,RS*)-2. The supernatants from crystallizations of (*SS,RR*)-**2**·$2CH_2Cl_2$ gave 70−64:30−36 (*SR,RS*)-**2**/(*SS,RR*)-**2** mixtures. Partial NMR data (THF-d_8, *SR,RS*): ^{1}H (δ) 1.69 (s, $C_5(CH_3)_5$); ^{13}C{^{1}H} (ppm) 100.65 (s, ***C***$_5(CH_3)_5$), 10.34 (s, C_5(***C***$H_3)_5$); ^{31}P{^{1}H} (ppm) 21.5 (br s).

(*SS,RR*)-2-$^{13}C_4$. This complex was prepared from **1**-$^{13}C_2$[61] by a procedure analogous to that for (*SS,RR*)-**2**. IR, Table 1; ^{13}C{^{1}H} NMR (ppm, C_6D_6/THF-d_8, ambient/-100 °C) 117.5/116.4 (dd, J_{CC} 97.2/98.1, 47.6/50.4 Hz, ReC***C***), 95.8/96.4 (ddd, J_{CC} 96.5/96.6, 47.1/50.2 Hz, J_{CP} 10.9/12.7 Hz, Re***C***); ^{31}P{^{1}H} NMR (ppm, THF-d_8, −95 °C) 22.0 (d, J_{CP} 14.5 Hz).

(*SS,RR*)-2^{2+}2PF$_6^-$. A Schlenk tube was charged with $Ag^+PF_6^-$ (0.024 g, 0.093 mmol) and toluene (5 mL). A solution of (*SS,RR*)-**2**·$2CH_2Cl_2$ (0.041 g, 0.028 mmol) in toluene (5 mL) was added dropwise by syringe with stirring. A deep blue precipitate formed immediately, which after 15 min was collected on a medium frit, washed with toluene (2 × 3 mL) and ether (3 × 2 mL), dried in air, and extracted with CH_2Cl_2 (5 mL). The extract was filtered through a Celite pad and concentrated to ca. 2 mL. Ether (7 mL) was added. The precipitate was isolated by filtration and dissolved in a minimum of CH_3CN. Toluene (8 mL) was added. The dark blue microcrystals were isolated by filtration and dried by oil pump vacuum to give (*SS,RR*)-**2**$^{2+}$$2PF_6^-$ (0.037 g, 0.024 mmol, 86%), mp 203−207 °C dec. Calcd for $C_{60}H_{60}F_{12}N_2O_2P_4Re_2$: C, 46.04; H, 3.86. Found: C, 45.91; H, 4.08. IR/Raman, Table 1; ^{1}H NMR (δ, CD_2Cl_2) 7.63−7.25 (m, $6C_6H_5$), 2.03 (s, $2C_5(CH_3)_5$); ^{31}P {^{1}H} NMR (ppm, CD_2Cl_2) 24.5 (br s) or 26.8/28.4 (s/s, 62:38, −93 °C); UV-vis (nm (ϵ, M^{-1} cm^{-1}), 2.9×10^{-5} M CH_2Cl_2) 234 (57 000), 270 sh (25 000), 392 (41 000), 574 (30 000); MS (positive FAB, 3-NBA/benzene)[60] 1276 (**2**$^+$, 100%), 638 (**2**$^{2+}$, 43%), 614 ((η^5-C_5Me_5)Re(NO)(PPh_3)$^+$, 80%); no other peaks above 460 of >15%.

(*SR,RS*)-2^{2+}2PF$_6^-$. This complex was prepared as 85−62:15−38 *SR,RS*/*SS,RR* mixtures from (*SR,RS*)/(*SS,RR*)-**2** mixtures by procedures analogous to that for (*SS,RR*)-**2**$^{2+}$$2PF_6^-$. Partial NMR data (*SR,RS*, CD_2Cl_2): ^{1}H (δ) 1.97 (s, $C_5(CH_3)_5$); ^{31}P{^{1}H} (ppm) 23.6 (br s) or 26.1/28.2 (s/s, 89:11, −93 °C).

(*SS,RR*)-2^{2+}-$^{13}C_4$ 2PF$_6^-$. This complex was prepared from (*SS,RR*)-**2**-$^{13}C_4$ by a procedure analogous to that for (*SS,RR*)-**2**$^{2+}$$2PF_6^-$. IR, Table 1; ^{13}C{^{1}H} NMR (ppm, CD_2Cl_2) 305.1 (ddd, J_{CC} 77.0, 40.7 Hz, J_{CP} 12.3 Hz, Re***C***), 213.5 (dd, J_{CC} 77.0, 40.7 Hz, ReC***C***), 133.4 (d, J_{CP} 15.3 Hz, *o*-Ph), 133.4 (s, *p*-Ph), 130.0 (d, J_{CP} 11.2 Hz, *m*-Ph), 114.3 (s, ***C***$_5(CH_3)_5$), 10.6 (s, C_5(***C***$H_3)_5$).

(*SS,RR*)-2$^{\bullet+}$PF$_6^-$. (**A**) A Schlenk tube was charged with (*SS,RR*)-**2**·$2CH_2Cl_2$ (0.080 g, 0.055 mmol) and toluene (3 mL). A solution of $Ag^+PF_6^-$ (0.014 g, 0.055 mmol) in toluene (2 mL) was added dropwise by syringe with stirring. A green-brown solid formed immediately and after 15 min was collected on a medium frit, washed with toluene (2

(58) (a) Thomas, J. A.; Jones, C. J.; McCleverty, J. A.; Collison, D.; Mabbs, F. E.; Harding, C. J.; Hutchings, M. G. *J. Chem. Soc., Chem. Commun.* **1992**, 1796. (b) Tolbert, L. M.; Zhao, X.; Ding, Y.; Bottomley, L. A. *J. Am. Chem. Soc.* **1995**, *117*, 12891.

(59) Zhou, Q.; Swager, T. M. *J. Org. Chem.* **1995**, *60*, 7096, and the introductory reference list therein.

(60) *m*/*z* for most intense peak of isotope envelope; relative intensities are for the specified mass range.

× 1 mL), and extracted with CH_2Cl_2 (5 mL). The extract was filtered through a Celite pad, and solvent was removed by oil pump vacuum. The residue was dissolved in a minimum of CH_3CN, and toluene (5 mL) was added. The solution was concentrated, and the dark green powder was collected on a medium frit, washed with ether, and dried by oil pump vacuum to give (*SS,RR*)-**2**$^{\bullet+}PF_6^-$ (0.054 g, 0.038 mmol, 69%). (**B**) A Schlenk tube was charged with (*SS,RR*)-**2**$^{2+}2PF_6^-$ (0.025 g, 0.016 mmol) and CH_2Cl_2 (3 mL). A solution of (*SS,RR*)-**2**$^{\bullet}2CH_2Cl_2$ (0.025 g, 0.017 mmol) in CH_2Cl_2 (3 mL) was added dropwise by syringe with stirring. The solution was concentrated to ca. 2 mL, and toluene (5 mL) was added. The solution was concentrated. The supernatant was decanted from the oily green precipitate, which was dissolved in a minimum of CH_2Cl_2. Ether (5 mL) was added. Solvents were removed by oil pump vacuum to give (*SS,RR*)-**2**$^{\bullet+}PF_6^-$ as a dark green powder (0.023 g, 0.016 mmol, 50%), mp 108−111 °C dec. Calcd for $C_{60}H_{60}F_6N_2O_2P_3Re_2$: C, 50.73; H, 4.26. Found: C, 50.72; H, 4.47. IR/Raman, Table 1; $^{31}P\{^1H\}$ NMR (ppm, THF-d_8, −80 °C) 23.0 (v br s); UV/vis/near-IR (nm (ϵ, M^{-1} cm^{-1}), 1.7 × 10^{-5} M CH_2Cl_2) 232 (60000), 270 sh (24000), 348 (24000), 454 sh (6400), 883 (15000), 1000 (9400), 1200 (3200); MS (positive FAB, 3-NBA/benzene)[60] 1276 (**2**$^+$, 81%), 642 (99%), 614 ((η^5-C_5Me_5)Re(NO)$(PPh_3)^+$, 100%); no other peaks above 310 of >33%.

(*SS,RR*)-2$^{\bullet+}$-$^{13}C_4$ PF_6^-. This complex was prepared from (*SS,RR*)-**2**-$^{13}C_4$ and (*SS,RR*)-**2**$^{2+}$-$^{13}C_4$ $2PF_6^-$ by a procedure analogous to method B for (*SS,RR*)-**2**$^{\bullet+}PF_6^-$. IR, Table 1.

Reductions of 2$^{\bullet+}$$PF_6^-$. A Schlenk flask was charged with (*SS,RR*)-**2**$^{\bullet+}PF_6^-$ (0.020 g, 0.014 mmol) and CH_2Cl_2 (5 mL). The solution was stirred for 4 h in the dark. Solvent was removed by oil pump vacuum, and a freshly prepared THF solution of sodium naphthalenide (0.015 mmol) was added dropwise. The brown solution was filtered through a Celite pad on a fritted funnel. Solvent was removed from the filtrate by oil pump vacuum to give crude **2** (0.017 g, 0.012 mmol). A ^{31}P NMR spectrum indicated ca. 85% purity (72% yield). Analysis by ^1H and ^{31}P NMR (-90 °C, THF-d_8) showed only (*SS,RR*)-**2**. An analogous experiment with a 65:35 (*SR,RS*)/(*SS,RR*)-**2**$^{\bullet+}PF_6^-$ mixture gave a 65:35 (*SR,RS*)/(*SS,RR*)-**2** mixture.

ESR. A 4 mm quartz tube was charged with a 7 × 10^{-3} M CH_2Cl_2 solution of (*SS,RR*)-**2**$^{\bullet+}PF_6^-$. Spectra were recorded on a Bruker ER 200D-SRC spectrometer (X-band frequency range, ambient temperature, modulation frequency 100 KHz). The magnetic field was calibrated immediately afterwards with diphenylpicrylhydrazide (g 2.0035 ± 0.0002) external standard, without changing the frequency of the microwave bridge. Second order corrections were applied.[62]

Cyclic Voltammetry. An EG&G Princeton Applied Research Model 273 potentiostat was employed. Cells were fitted with Pt working (2.0−1.6 mm^2) and counter electrodes and a Ag wire pseudoreference electrode. All CH_3CN solutions were 2−5 × 10^{-3} M in **2**, 0.1 M in $Et_4N^+ClO_4^-$ (dried by oil pump vacuum, 70 °C), and prepared under argon. All CH_2Cl_2 solutions were 2−8 × 10^{-3} M in **2**, 0.1 M in *n*-$Bu_4N^+BF_4^-$ (crystallized from ethanol/hexane and dried by oil pump vacuum), and prepared under nitrogen. Ferrocene was subsequently added,[25] and calibration voltammograms recorded. The ambient laboratory temperature was 22.5 ± 1 °C.

Crystallography. Data were collected on dark red or blue prisms of (*SS,RR*)-**2**$^{\bullet}2CH_2Cl_2$ or (*SS,RR*)-**2**$^{2+}$ $2PF_6^-$ (from CH_2Cl_2/ether, vapor diffusion) per Table 2. Cell constants were obtained from 25 reflections with 10° < 2θ < 20° and 15° < 2θ < 25°, respectively. Space groups were determined from systematic absences (none and *h*0*l*, *l* = 2*n*, 0*k*0, *k* = 2*n*) and subsequent least-squares refinement. Lorentz, polarization, and empirical absorption (Ψ scans) corrections were applied. Structures were solved by standard heavy-atom techniques with the SDP or MOLEN VAX packages. The latter was refined with SHELXL-93.[63] Non-hydrogen atoms were refined with anisotropic thermal parameters. Hydrogen atom positions were calculated and added to the structure factor calculations, but were refined only for (*SS,RR*)-**2**$^{2+}2PF_6^-$ (riding model). Scattering factors, and $\Delta f'$ and $\Delta f''$ values, were taken from the literature.[64] Other data are given in the Supporting Information (−100 °C structure) and the Supporting Information of a communication (16 °C structures).[12a]

Computations. The geometry optimizations were carried out at the HF level of theory using a quasi-relativistic effective (small) core potential (ECP) for rhenium.[65] The rhenium $5s^2$ and $5p^6$ electrons were treated explicitly as part of the valence space. A (441/2111/21) split-valence basis set was used for the 15 outercore and valence rhenium electrons. A 6-31G(d) all electron basis set was used for hydrogen, carbon, nitrogen, and oxygen, while a pseudopotential with a (31/31/1) valence basis set was used for phosphorus and chlorine.[66] The d polarization functions have five spherical components. This basis set combination is our standard basis set II.[67] The geometry optimizations of (Cl)Re(NO)(PH_3)(CCCC)(H_3P)(ON)Re(Cl) (**2′**) and **2′**$^{2+}$ were carried out without symmetry constraints, except that phosphorus-hydrogen distances were forced to be the same. Numerical frequency calculations of **2′** and **2′**$^{2+}$ were not conducted for computational reasons. Since optimizations were performed in C1 symmetry, structures are believed to be potential energy surface minima. Vibrational frequency calculations were carried out for hydrocarbon substrates, and their optimized geometries are energy minima. The calculations employed the program packages Gaussian 92[68a] and Gaussian 94.[68b] The electron density distribution $\rho(\mathbf{r})$, gradient vector field $\nabla\rho(\mathbf{r})$, and associated Laplacian $\nabla^2\rho(\mathbf{r})$ calculations used the programs PROAIM, SADDLE, GRID, and GRDVEC.[69]

Acknowledgment. This work was supported by the NSF, DFG (Sonderforschungsbereich 260 and Graduiertenkolleg "Metallorganische Chemie"), Fonds der Chemischen Industrie, and Alexander von Humboldt Foundation. We thank Dr. R. S. McLean (duPont) for magnetic susceptibility measurements, Professors J. S. Miller (Utah) and C. Lapinte (Rennes) for helpful discussions, and the HRZ Marburg, HHLRZ Darmstadt, and HLRZ Jülich for excellent service.

Note Added in Proof. A series of RuC_4Ru complexes with (η^5-C_5H_5)Ru(PPh_3)(L) endgroups has recently been reported. These can be generated in as many as *five* oxidation states and have been isolated in three: Bruce, M. I.; Denisovich, L. I.; Low, P. J.; Peregudova, S. M.; Ustynyuk, N. A. *Mendeleev. Commun.* **1996**, 200.

Supporting Information Available: Tables of atomic coordinates and anisotropic thermal parameters (−100 °C) for (*SS,RR*)-**2**$^{2+}2PF_6^-$ (4 pages). See any current masthead page for ordering and Internet access instructions.

JA9631817

(61) This complex was prepared analogously to the unlabeled compound.[17] $^{13}C\{^1H\}$ NMR (ppm, THF-d_8) 111.1 (d, J_{CC} 121 Hz, ReC***C***), 98.0 (dd, J_{CC} 121 Hz, J_{CP} 16 Hz, Re***C***).

(62) Goodman, B. A.; Raynor, J. B. *Adv. Inorg. Chem. Radiochem.* **1970**, *13*, 135, 221.

(63) (a) Frenz, B. A. in The Enraf-Nonius CAD 4 SDP − A Real-time System for Concurrent X-ray Data Collection and Crystal Structure Determination, In *Computing and Crystallography*; Schenk, H., Olthof-Hazelkamp, R., van Konigsveld, H., Bassi, G. C., Eds.; Delft University Press: Delft, Holland, 1978: pp 64−71. (b) Sheldrick, G. M. *SHELXS-93*; University of Göttingen, 1993. (c) Sheldrick, G. M., manuscript in preparation for *J. Appl. Cryst*.

(64) Cromer, D. T.; Waber, J. T. In *International Tables for X-ray Crystallography*; Ibers, J. A., Hamilton, W. C., Eds.; Kynoch: Birmingham, England, 1974; Volume IV, Tables 2.2B and 2.3.1.

(65) Hay, P. J.; Wadt, W. R. *J. Chem. Phys.* **1985**, *82*, 299.

(66) Bergner, A.; Dolg, M.; Küchle, W.; Stoll, H.; Preuss, H. *Mol. Phys.* **1993**, *80*, 1431.

(67) Frenking, G.; Antes, I.; Böhme, M.; Dapprich, S.; Ehlers, A. W.; Jonas, V.; Neuhaus, A.; Otto, M.; Stegmann, R.; Veldkamp, A.; Vyboishchikov, S. F. In *Reviews in Computational Chemistry*; Lipkowitz, K. B., Boyd, D. B., Eds.; VCH: New York, Vol. 8, pp 63−144.

(68) (a) Frisch, M. J.; Trucks, G. W.; Head-Gordon, M.; Gill, P. M. W.; Wong, M. W.; Foresman, J. B.; Schlegel, H. B.; Raghavachari, K.; Robb, M. A.; Binkley, J. S.; Gonzalez, C.; Martin, R.; Fox, D. J.; DeFrees, D. J.; Baker, I.; Stewart, J. J. P.; Pople J. A., Gaussian Inc., Pittsburgh, PA 1992. (b) Frisch, M. J.; Trucks, G. W.; Schlegel, H. B.; Gill, P. M. W.; Johnson, B. G.; Robb, M. A.; Cheeseman, J. R.; Keith, T. A.; Petersson, G. A.; Montgomery, J. A.; Raghavachari, K.; Al-Laham, M. A.; Zakrzewski, V. G.; Ortiz, J. V.; Foresman, J. B.; Cioslowski, J.; Stefanov, B. B.; Nanayakkara, A.; Challacombe, M.; Peng, C. Y.; Ayala, P. Y.; Chen, W.; Wong, M. W.; Andres, J. L.; Replogle, E. S.; Gomberts, R.; Martin, R. L.; Fox, D. J.; Binkley, J. S.; Defrees, D. J.; Baker, I.; Stewart, J. J. P.; Head-Gordon, M.; Gonzalez, C.; Pople, J. A. Gaussian Inc.: Pittsburgh, PA, 1995.

(69) Biegler-König, F. W.; Bader, R. F. W.; Tang, T.-H. *J. Comput. Chem.* **1982**, *3*, 317.